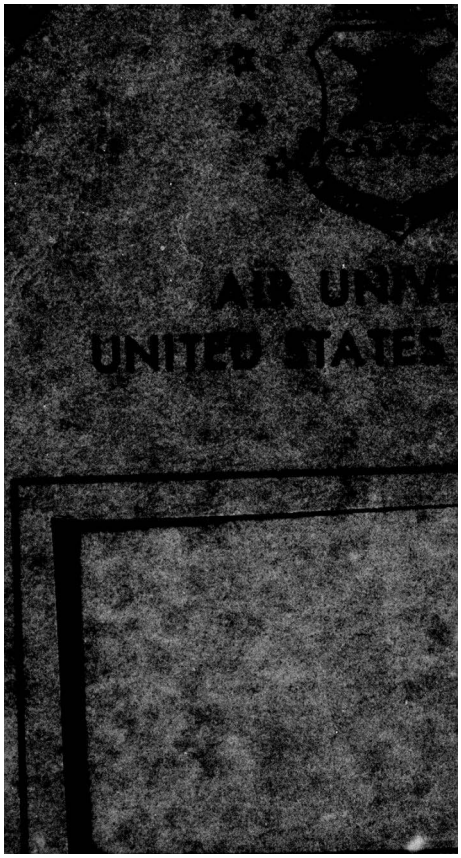
AD-A039 162 AIR FORCE INST OF TECH WRIGHT-PATTERSON AFB OHIO SCH--ETC F/G 13/13
CUTOUT REINFORCEMENT OF STIFFENED CYLINDRICAL SHELLS.(U)
MAR 77 J A CERVANTES

UNCLASSIFIED AFIT-GAE/MC/76D-2 NL

1 OF 2
ADA
039162




AIR UNIV
UNITED STATES

GAE/MC/76D-2

DDC
RECEIVED
MAY 10 1977
C

CUTOUT REINFORCEMENT

OF

STIFFENED CYLINDRICAL SHELLS

THESIS

GAE/MC/76D-2 J. Anthony Cervantes

ACCESSION for
NTIS White Section
DDC Buff Section
UNANNOUNCED
JUSTIFICATION
BY
DISTRIBUTION/AVAILABILITY CODES
Dist. AVAIL. and/or SPECIAL

Approved for public release; distribution unlimited

(See Form 1473)

GAE/MC/76D-2

CUTOUT REINFORCEMENT OF STIFFENED CYLINDRICAL SHELLS

THESIS

Presented to the Faculty of the School of Engineering
of the Air Force Institute of Technology
Air University
in Partial Fulfillment of the
Requirements for the Degree of
Master of Science

by

J. Anthony Cervantes
Graduate Aeronautical Engineering

March 1977

Approved for public release; distribution unlimited.

Preface

I am sincerely grateful to Dr. Anthony Palazotto for the long hours he has spent guiding and instructing me for this project.

I wish to thank my wife, Jane, for her patience and encouragement while I was attending AFIT. Her tolerance and hard work while she was typing this thesis are deeply appreciated.

J. Anthony Cervantes

Contents

	Page
Preface	ii
List of Figures	iv
Symbols	vi
Abstract	ix
I. Introduction	1
Background	1
Purpose	24
General Procedure	24
II. Theory and Modeling	25
General Description of STAGS	25
Outline of STAGS Theory	26
Modeling	33
III. Results	35
Model Description	35
Numerical Results	44
IV. Conclusions	70
Bibliography	72
Appendix A: Reinforcing Frame Geometric Parameters	74
Appendix B: Buckling Loads and Buckling Load Ratios	79
Vita	83

List of Figures

Figure		Page
1.	Shell Geometry and Sign Convention	3
2.	Definition of Initial Postbuckling Slope	13
3.	Basic Shell Geometry	36
4.	Smeared Stiffner Geometry and Spacing	38
5.	Reinforcing Frame Locations	40
6.	Finite Difference Meshes	42
7.	Boundary Conditions	43
8.	P_{cr}/P_o vs d For a Stringer Stiffened Shell, 2a = 12"	45
9.	P_{cr}/P_o vs d For a Stringer Stiffened Shell, 2a = 24"	46
10.	P_{cr}/P_o vs d For a Ring and Stringer Stiffened Shell, 2a = 12"	47
11.	P_{cr}/P_o vs d For a Ring and Stringer Stiffened Shell, 2a = 24"	48
12.	Linear Displacements For a Stringer Stiffened Shell, 2a = 24"	50
13.	Linear Displacements For Run 29	51
14.	Linear Displacements For a Stringer Stiffened Shell, 2a = 12"	52
15.	Linear Displacements For Run 1	53
16.	Linear Displacements For Run 4	54
17.	S_x For a Stringer Stiffened Shell 2a = 12"	56
18.	S_x For Run 1	57
19.	S_x For Run 4	58
20.	Normalized Buckling Displacements For a Stringer Stiffened Shell, 2a = 12"	59
21.	Normalized Buckling Displacements For Run 1	60

Figure		Page
22.	Normalized Buckling Displacements For Run 4 . . .	61
23.	Normalized Buckling Displacements For Run 6 . . .	63
24.	P_{cr}/P_o vs W_{sf}/W_o For a Stringer Stiffened Shell, 2a = 12".	64
25.	P_{cr}/P_o vs W_{sf}/W_o For a Stringer Stiffened Shell, 2a = 24".	65
26.	P_{cr}/P_o vs W_{sf}/W_o For a Ring and Stringer Stiffened Shell, 2a = 12"	66
27.	P_{cr}/P_o vs W_{sf}/W_o For a Ring and Stringer Stiffened Shell, 2a = 24"	67

Symbols

a	hole radius or half width of square cutout
A, B	component matrices of $L'_{\lambda X_L}$
A_1, b_1, b_{str}, h_{str}	geometric properties for the stringers
A_2, b_2, b_r, h_r	and rings shown in Figure 4.
A_{sf}, b_{sf}, h_{sf},	geometric properties of the rein-
$I_{x \text{ or } y}$, I_z	forcing frame given in Appendix B.
A_{jk}	displacement series coefficients
$d = L_{sf}$	= distance of frame from the centerline of the cutout
D	plate stiffness $Eh^3/12(1-nu^2)$
D^i	strain energy density matrix
e_x, e_θ, $e_{x\theta}$	strains
E	modulus of elasticity
F	vector of external forces
F_L	vector of external forces for linear solution
G	shear modulus
h	shell thickness
i_{max}	total number of mesh stations
K_x, K_θ, $K_{x\theta}$	curvature changes
L	length of the shell
L_x^*, L_y^*	wavelengths in the x and θ directions
L	in Eq. (18) is a non-linear "stiffness" operator
L'_{X_k}	is special derivative of L as defined in Eq. (22)
m	number of half waves in the axial direction
mu	wavelength ratio m/n
mu'	$\frac{1}{2}(12(1-nu^2)^{\frac{1}{4}} \ (a^2/Rh)^{\frac{1}{2}}$
M_x, M_θ, $M_{x\theta}$	moment resultants

n	number of full waves in the circumferential direction
nu	Poisson's ratio
N	wavelength parameter
N_x, N_θ, $N_{x\theta}$	stress resultants
P_x, P_θ, P_r	dead loads in x, θ, and z directions
P_o	buckling load of shell without a cutout and without a reinforcing frame
P_1	buckling load of shell with a cutout but without a reinforcing frame
P_{cr}	buckling load
s	imperfection sensitivity angle
S_{cl}	classical buckling stress $\approx .6Eh/R$
S_{cr}	critical buckling stress
u, v, w	displacements in the axial, circumferential, and radial directions, respectively
u^*, v^*, w^*	displacements at buckling
u^i, v^i, w^i	displacements at mesh station i
U	total strain energy
ΔU	strain energy density at mesh station i
V	total potential energy
W	potential energy of the work done by the external forces F
WOA	volume per unit area of the removed cutout material
W_{sf}/W_o	ratio of the reinforcing frame volume to the volume of the removed cutout material
x, θ, z	the coordinates in the axial, circumferential and radial directions, respectively

X	vector of "raw" displacements
X_L	vector of "raw" displacements for the linear solution
Y	bifurcation displacement vector
Z	Batdorf shell parameter $(1-nu^2)^{\frac{1}{2}}$ (L^2/Rh)
Z^i	vector of strains and rotational changes at mesh station i
λ	eigenvalue of det $(L'_{\lambda X_L}) = 0$

ABSTRACT

A study was carried out to determine the optimum placement and volume of a reinforcing frame around a cutout in an axially loaded stringer and ring and stringer stiffened cylindrical shell. The problem was analyzed using the linear bifurcation portion of STAGS (Structural Analysis of General Shells). Four parameters were varied; stringers versus rings and stringers, cutout size, ratio of frame volume to cutout volume, and frame position. It appeared that in most cases the position with the frame next to the cutout edge was the most effective. This can be attributed to the frame's ability to delay the onset of local buckling. However, there was a relative maximum in the frame distance versus critical load curves for a frame positioned away from the cutout edge at a low ratio of frame to cutout volume.

CUTOUT REINFORCEMENT OF STIFFENED CYLINDRICAL SHELLS

I. Introduction

Background

The cylindrical shell is an important aerospace structural element. The semi-monocoque airplane shell structure of the 1930's was typified by a very thin skin supported by much stiffer longitudinal and tranverse reinforcing members. As a result, buckling of the thin skin panels was primarily a local phenomenon. With the advent of missles and the increase in flight speed, aircraft skins have become thicker, and skins and reinforcement are of similar rigidity. Buckling changed from a local characteristic to a problem of general shell instability. A further complication is encountered when an access door or similar hole must be inserted in the structure, thus weakening an otherwise very efficient structure. The purpose of this thesis is to determine the strengthening effects of a reinforcement around a rectangular cutout in a stiffened cylindrical shell.

First, a history of the buckling of cylindrical shells is presented to put this problem in its proper context.

Lorenz (Ref 1) was the first to derive a buckling

formula for an axially compressed cylindrical shell. He assumed that the edges were simply supported and that both the prebuckling and buckling deformations were axisymmetric. His equations were slightly inaccurate, however. Timoshenko (Ref 2) published the correct classical buckling equation in 1910. The classical buckling formula is:

$$S_{cl} = (3(1-nu^2))^{-\frac{1}{2}} E(h/R) \cong .6E(h/R) \qquad (1)$$

where S_{cl} is the classical buckling stress.

The general case of buckling without restriction to axial symmetry of the buckling deformations was first discussed by Lorenz in 1911, assuming that displacements in an axial direction were negligibly small and the boundary conditions were:

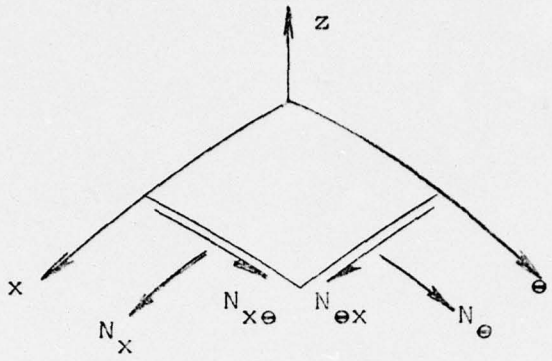
$$v^* = w^* = M_x = 0 \qquad (2)$$

The coordinate system used in this thesis is shown in Fig. 1.

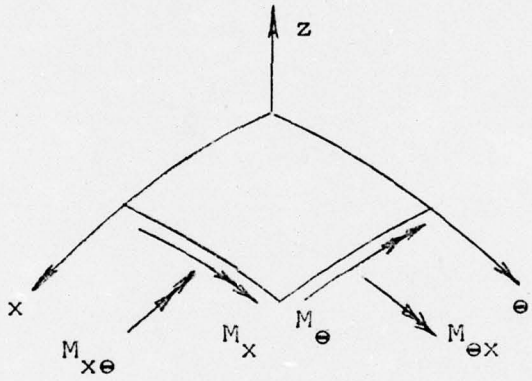
The buckling displacements are u^*, v^*, and w^* in the axial, circumferential and radial directions, respectively. The coordinate directions are x, e, and z.

In 1914, Timoshenko (Ref 2) determined that the non-axisymmetric buckling stress was equal to .6E(h/R), the same value obtained for the classical axisymmetric case. For non-axisymmetric buckling, theory predicts the entire surface will be covered by relatively small buckles. This buckling pattern will be referred to as either the chessboard pattern or the diamond pattern.

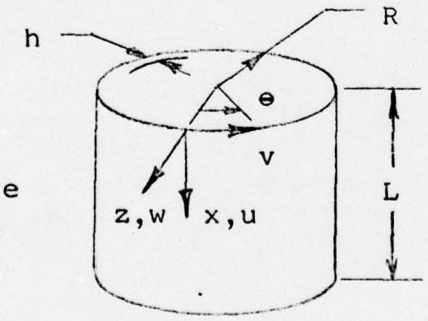
There are two basic problems with the buckling patterns predicted by the linear classical theory. The first is that



Stress Resultants



Moment Resultants



Shell Geometry

Note:
u*, v*, and w* are the displacements u, v, and w at buckling

Figure 1. Shell Geometry and Sign Convention

axially symmetric buckling can occur only when there is some plasticity, while classical buckling theory assumes perfect elasticity. The second problem is that the uniform pattern of buckles in chessboard buckling, is observed in experiments as only one or two rows of buckles with the remainder of the shell smooth.

In 1932 Flugge (Ref 1) tested a number of celluloid cylinders for a variety of length to radius ratios and radius to wall thickness ratios. He discovered that these buckled at stresses considerably below those predicted by the classical buckling equation, with experimental to theoretical buckling stress ratios ranging from .52 to .65. To determine the possible causes of the discrepancy between experiment and theory, Flugge examined the effect of boundary conditions and small geometric imperfections upon the buckling stress.

In the classical approach to shell instability, the shell was assumed to expand uniformly inthe radial direction along the shell's entire length due to the applied axial load. Flugge solved for the axially symmetric deformations of a shell whose end sections are restrained in the radial direction. He found that a curved region existed along the meridian near the ends. Increased loading caused the curved regions to extend toward the middle and eventually the radial displacements became infinitely large at the critical load. He noted that the curvature caused local stress to exceed the elastic limit even if S_{cr} was well below the elastic limit. In his

investigation of a sine wave deviation from perfect circular cylindrical form, Flugge determined that the imperfection would dominate the buckling and grow infinitely large as the classical load was approached.

Another investigation into the effect of boundary conditions was given by Hoff in (Ref 3) and outlined in (Ref 1). Starting from equations by Nachbar for a pressurized spherical shell, Hoff was able to determine that a semi-infinite shell with the near edge perfectly free to displace would buckle axisymmetrically at one-half the classical buckling stress. In a follow up paper by Nachbar and Hoff, S_{cr}/S_{cl} was determined to be .38 for non-axisymmetric buckling.

For many years, the biggest problem with the solution of shell buckling was the complexity of the governing shell equations. In 1933, Donnell (Ref 4) formulated equilibrium equations for a cylindrical shell under torsion, based on the following assumptions:

1. The material is perfectly elastic.
2. The thickness is small compared to the radius.
3. The deflections are small compared to the thickness.
4. Neglect distortion due to transverse shear.

A more convenient form of Donnell's small displacement equations (Ref 5) allowing general loading are:

$$\begin{aligned} RN_{x,x} + N_{x\,\theta,\theta} &= p_x \\ RN_{x\theta,x} + N_{\theta,\theta} &= p_\theta \\ D\,\nabla^4 w + N\theta/R &= p_r \end{aligned} \qquad (3)$$

The applied loads are p_x, p_θ, and p_r in the axial, circumferential, and radial directions, respectively.

The Donnell equations have the advantage that they are much simpler than most others and yet, they are sufficiently accurate in buckling problems if the number of waves around the circumference is sufficiently large. In 1947, Batdorf (Ref 6) used these equations to solve a variety of stability problems, and compared the solutions with other theoretical solutions and test results.

Using the Donnell equations, Hoff (Ref 1) demonstrated that the appropriate boundary conditions for the classical case of buckling are:

$$w^* = w^*_{,xx} = N_x = v^* = 0. \tag{4c}$$

This is not the only possible simple support condition. The four simple support conditions proposed by Hoff are (Ref 1):

SS1	$w^* = 0$	$w^*_{,xx} = 0$	$N_x = 0$	$N_{x\theta} = 0$
SS2	$w^* = 0$	$w^*_{,xx} = 0$	$u^* = 0$	$N_{x\theta} = 0$
SS3	$w^* = 0$	$w^*_{,xx} = 0$	$N_x = 0$	$v^* = 0$
SS4	$w^* = 0$	$w^*_{,xx} = 0$	$u^* = 0$	$v^* = 0$

(4)

The corresponding clamped end conditions are:

RF1	$w^* = 0$	$w^*_{,x} = 0$	$N_x = 0$	$N_{x\theta} = 0$
RF2	$w^* = 0$	$w^*_{,x} = 0$	$u^* = 0$	$N_{x\theta} = 0$
RF3	$w^* = 0$	$w^*_{,x} = 0$	$N_x = 0$	$v^* = 0$
RF4	$w^* = 0$	$w^*_{,x} = 0$	$u^* = 0$	$v^* = 0$

(5)

In this notation classical simple supports correspond to SS3.

In the next few years researchers investigated both semi-infinite and finite length shells with various edge conditions with the aid of Donnell's small displacement equations; and the results compared well with other accepted, but tedious solutions.

The significance of these results indicated that there were solutions other than the classical one for the buckling of a thin walled circular cylinder under axial compression, despite the fact that the problem was governed by linear equations. Another important aspect these solutions pointed out, was that a thin shell placed between the platens of a testing machine can buckle anywhere between one-half and the full value of the classical buckling stress. The exact value depends on the friction between the test article and the platen.

The difference between the predictability of the buckling stress of bars and plates and thin shells had puzzled Von Karmen. He observed that buckles grew gradually in bars and plates, but snap through in shells. After buckling, bars and plates carried the load; while shells could only carry a fraction of the buckling load. He determined that the key lay in the curvature of the shell. The classical solution implies that the surface may buckle inward or outward with equal ease. However, real shells show a preference to buckle inward. In 1934 Donnell (Ref 7) remedied this problem by adding terms that were non-linear in the displacements which took into

account the non-linear effects of the shell curvature. The non-linear Donnell large displacement equations (Ref 5) in a convenient form are:

$$RN_{x,x} + N_{x\theta,\theta} = P_x$$

$$RN_{x\theta,x} + N_{\theta,\theta} = P_\theta$$

$$D\nabla^4 w^* + N\theta/R - (N_x w^*_{,xx} + 2N_{x\theta} w^*_{,x\theta}/R + N_\theta w^*_{,\theta\theta}/R) = P_r \quad (6)$$

Note that the linear Donnell small displacement Eqs. (3) may be obtained from the non-linear Donnell large displacement Eqs. (6) by the simple omission of all terms non-linear in u, v, and w.

The problem with these equations was that they were non-linear partial differential equations and could not be solved exactly. Both Von Karmen and Donnell obtained rigorous solutions for these equations by assuming displacement patterns. In 1942, Tsien suggested replacing the buckling stress with the minimum equilibrium stress after buckling as being reasonable for buckling purposes.

While others were working on physical and mathematical reasons for the strange behavior of axially compressed cylindrical shells, Yoshimura (Ref 1) found a geometric reason for this behavior. In 1951, Yoshimura determined that a circular shell could buckle into a diamond pattern similar to the previously mentioned chessboard pattern without causing any membrane stresses. The significance of this pattern is that a thin shell's extensional stiffness is much greater than its bending stiffness. The

incompatibility of the diamond pattern with the support condition probably is the reason why, experimentally, shells buckle with only one or two rows of diamonds.

In 1963, Almroth (Ref 1) using the computer investigated combinations of the various terms of the series:

$$w^* = \sum_{j=0}^{\infty} \sum_{k=0}^{\infty} A_{jk} \cos (j\pi x^*/L_x^*) \cos (k\pi \theta^*/L_y^*) \qquad (7)$$

In this investigation, Almroth minimized the total potential energy with respect to mu and N where:

$$mu = m/n \qquad N = n^2(h/R) \qquad (8)$$

m is the number of half waves in the axial direction and n is the number of full waves in the circumferential direction. Almroth's results were in excellent agreement with work by Thielemann (Ref 1), who had performed experiments with extreme care and later compared the experimental results with analytical results.

The problem of considering various combinations of terms in Eq. (7) was looked at by several authors between 1941 and 1965. The minimum $S_{cr}R/Eh$ determined from these efforts was .0427, which was well below the classical value of .6.

It is interesting to note that with the larger number of terms retained in the expression for w^*, the coefficients of the double Fourier series approach those for a Fourier series expansion of the Yoshimura buckling pattern. A problem with the technique whereby the potential energy was minimized with respect to the wave length parameters was that, as the number of terms increased, the

solution was only valid for an infinitely thin shell, since N was found to approach zero. This was overcome by requiring $N \geq 4n/R$, since n, the number of circumferential waves could not be less than two.

Investigations based on the Donnell large displacement equations, were carried out by several authors in the next few years to determine analytically the effect of small deviations from the nominal geometry upon the buckling load of a thin cylindrical shell. It was noted by Madsen and Hoff (Ref 1) that a non-symmetric deviation amounting to one-tenth the wall thickness coupled with an amplitude of axisymmetric deviations one-fortieth the thickness of shell resulted in a reduction of maximum load to 60 per cent of the classical value for a perfect shell.

Hoff noted that the large displacement Donnell equations were completely inadequate to represent the inextensional deformations of Yoshimura pattern when there are five to ten triangles around the circumference of the shell. Mayers & Rehfield (Ref 1) also noted that the equations could not handle the plastic stresses along the triangle edges with the result that the curvature predicted along the triangle edges was too large.

Another limitation of the theory is that it does not adequately express the reduction of the buckling stress due to large R/h. Theory predicts that k is independent of R/h in $S_{cr} = k\ Eh/R$ (for S_{cl}, $k = .6$). It was noted by Mayers and Rehfield that the dependence of k on R/h was negligibly

small even using the Donnell large displacement equations.

Madsen & Hoff (Ref 1) demonstrated that the replacement of the grossly inadequate large displacement Donnell equations by more accurate equations does not significantly change the equilibrium stresses obtainable from the equations. The explanation of the apparent paradox is that the large number of buckles around the circumference allow the shell to be considered a shallow shell.

Stein, Fischer, and Almroth separately investigated the effect of prebuckling displacements on the buckling stress for a variety of boundary conditions. Almroth compared the results and concluded that the effect of boundary conditions was much larger than the effect of prebuckling displacements.

Koiter was the first to call attention to the importance of the stability of the system at the bifurcation itself. He demonstrated that if the second derivative of the potential energy was zero, and if the third derivative were not, then the system would be unstable. This is true since the bifurcation point would correspond to a minimax of the potential energy. Under such circumstances the system is very sensitive to small initial deviations from the perfect shape.

Stein (Ref 8) presented an excellent survey of advances in shell buckling during the time period of 1960-1967. In this paper, Stein dealt with two major topics: The impact of improved non-linear shell prebuckling theory and the

significance of experiments upon near-perfect shell specimens.

Stein gave a brief derivation of consistent shell buckling equations to point out the differences between consistent and conventional buckling theory. In conventional theory, linear membrane theory is assumed to apply in the prebuckling range which leads to constant radial displacements. This in turn assumes that the shell boundary conditions change during buckling. On the other hand, in consistent buckling theory the non-linear large deflection Donnell equations, Eqs. (6), are used so that the prebuckling boundary conditions can be consistent with the boundary conditions for the buckling solution. It should be noted that the buckling equations for consistent theory involve prebuckling terms which would vanish in conventional theory.

Stein picked results from several researchers who had tested near-perfect shells. The materials used were photoplastic, nickel, and copper. The importance of these tests was that the near-perfect shells buckled at stresses considerably closer to the classical buckling stress than previous experiments. The conclusion was that most of the scatter in experimental results was due to small initial deviations from perfect shell geometry.

The use of non-linear bending theory has lead to closer agreement between theory and experiment, particularly for a near-perfect shell with R/h less than 300; see figure 1 (Ref 8).

Stein also includes a section on shallow spherical shells under external pressure with similar improved agreement between theory and experiment.

Practical shells do not have near-perfect geometry as assumed by theory and therefore, techniques to determine the reduction in buckling strength due to imperfections are required. Artificial buckling criteria such as post-buckling minimum loads and loads corresponding to equal energy states do not account for imperfections, and are thus inadequate.

A measure of a shell's sensitivity to initial imperfections is given by the imperfection sensitivity angle s (Ref 8). This parameter is related to the initial post-buckling slope of the load vs characteristic displacement curve, and is defined in Fig. 2 taken from (Ref 8). The

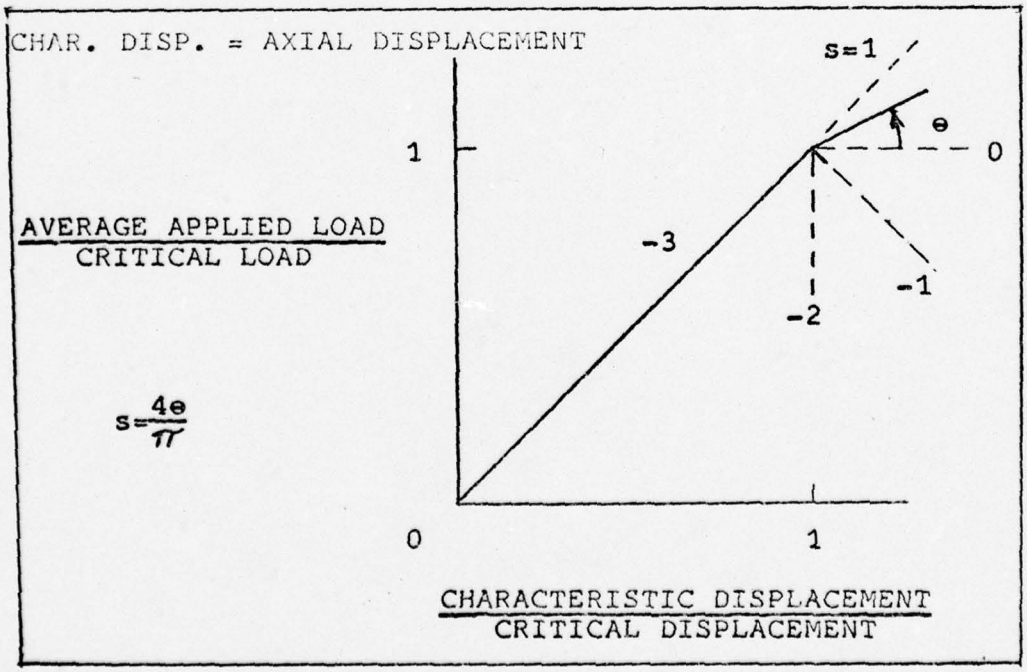


Figure 2. Definition of Initial Postbuckling Slope

parameter s varies from -3 to 1, that is from a condition where it doubles back on itself to a condition where it is tangent to the prebuckling curve. For s positive, imperfections do not appreciably alter the buckling load; for s negative, imperfections will decrease the buckling load. s also provides a measure of the expected violence of the buckling process; for $s<-2$ "snap through" buckling will always occur, whereas for $-2<s<0$ buckling will be violent or gentle depending on whether loading or characteristic displacement is controlled.

For the cylinder in axial compression the sensitivity angle s (calculated on the basis of conventional theory) is $s = -3$. This condition agrees with snap through buckling observed in experiments.

Although it has been previously pointed out that the major cause of disagreement between experiment and theory is the presence of initial defects, research indicates that boundary conditions, eccentricity of stiffening and eccentricity of load application also affect the buckling load.

The eccentricity of stiffeners also strongly affects the buckling load. For example, Card (Ref 1) demonstrated that externally stiffened shells have carried more than twice the load by internally stiffened cylindrical shells. This effect will be covered more extensively in a later section.

Another factor which affects the buckling load, is the eccentricity of the loading relative to the neutral

axis. Results obtained by Block and Almroth (Ref 1) show that up to four times the load are available with the load applied on the inside of the neutral surface for both internal and external stiffening compared to the cases for loading at the neutral surface.

An aspect of stiffened cylindrical shells that is not present in the unstiffened shell, is that small meridianal curvature drastically affects the buckling load. For internal stiffening, the addition of 7.8 per cent outward rise results in an increase in load by a factor of nine. Unstiffened shells in compression do not carry appreciably more load with the addition of small meridianal curvature.

The conclusion that can be drawn is that properly posed buckling theory is correct; and that there is no need for postbuckling minimums.

In the application of thin shell technology for aerospace applications, it is often necessary to design a cylindrical shell with a cutout for non-structural access doors to internal equipment, or any of a number of other purposes. The exact solution to such a problem is beyond present analytical capabilities. As a result, several researchers have undertaken projects in this area. One of these researchers is Starnes (Ref 9), who has investigated the buckling of a thin unstiffened cylindrical shell with a single cutout, both experimentally and theoretically.

Starnes (Ref 9) conducted two series of experiments, one on shells made of Dupont's Mylar with a lap seam; and

the other series of tests on seamless electroformed copper shells. The parametric ranges were: $400<R/h<960$ and $0<a/R<.5$; where a was the hole radius. The experimental buckling loads, displacements, and the stress distribution applied at the end of the shell were correlated with a theoretical parametric study performed by means of a Rayleigh-Ritz type of approximation. The results of these experiments led to the conclusion that the governing parameter of the problem was related to a^2/Rh rather than a/R as suggested by Tennyson. Lekkerkerker (Ref 9) has shown that the parameter:

$$mu' = \tfrac{1}{2}\,(12(1-nu^2))^{\frac{1}{4}}\,(a^2/Rh)^{\frac{1}{2}} \qquad (9)$$

governs the prebuckling stress distribution and displacements for a circular cylinder with a circular hole in its side. It should be noted that the effect of the hole is very localized in nature. Both membrane and bending stress increments occur; but the bending stress increment is always much less than the membrane stress increment. It should be appreciated that the maximum membrane stress will rise significantly above the stress value obtained for a hole in a flat plate.

The buckling analysis referred to later and the experimental results presented below indicate that the buckling load of a circular cylinder with a circular hole in its side are related to the ratio a^2/Rh. It is reasonable to assume that mu' of Eq. (9) is the governing parameter for the problem.

It was possible to identify approximate ranges of the parameter mu' with different buckling characteristics. For mu' $\leq$ .4 imperfections were the dominating factor causing buckling below the classical load. For values of mu' between .4 and 1.0 the buckling loads dropped sharply as mu' increased. In this range, the prebuckling stress concentration around the hole caused local buckling, and since the entire shell was sensitive to small disturbances in this load range, general buckling was caused by the local snap through. For mu' between 1. and 2.0 there is a transition between the sharp decline in buckling load of the previous region and the milder decline beyond mu' = 2.0. For mu' greater than 2 local buckling occurred at a low enough load so that the shell was not sufficiently sensitive to disturbances to cause general collapse. The collapse load was in general slightly higher than the local buckling load for mu' $>$ 2. For this case, the maximum displacement at the edge of the hole was on the order of .25 inch, which is many times the wall thickness, and surprisingly large when compared to the prebuckling displacements in a cylinder without a cutout.

Starnes (Ref 9) presents results from his copper shell experiments for the range 0 $\leq$ mu' $\leq$ 3. The resulting curve of S/S_{cl} vs mu' followed very nicely with the data from the Mylar shells. Of interest are figures 6 and 7 in (Ref 9) representing the prebuckling displacements at S/S_{cl} = .398. Starnes performed

a simplified analysis of the buckling of a circular cylindrical shell with a single circular hole assuming that general collapse was initiated by local buckling and that the stress distribution in a flat plate closely resembled the membrane stress distribution in a cylinder. Despite these restrictive assumptions, the trend indicated by the analysis followed the experimental results for mu' < 2.5. For mu' > 2.5 the Donnell approximations of linear shell theory were no longer valid due to the large prebuckling displacements and theory and experiment diverged sharply.

As previously mentioned, local buckling is rarely critical in modern stiffened shells and hence general instability is the dominant criterion. For many years stability analyses of stiffened shells considered equivalent orthotropic shells and the eccentricity of the stiffeners was not taken into account in these analyses, due to the complexity of the equations. More recently with the aid of computers the effect and influence of stiffener eccentricity has been explored by authors for internal and external stiffening for both rings and stringers. The general conclusion that can be drawn is that for an axially loaded cylinder, external stiffening is most efficient. A simplified approach to the problem of incorporating eccentric stiffening into the shell equations is called smeared stiffener theory in which the stiffeners are assumed to be evenly distributed or "smeared" over the entire shell surface. This approach appears to be satisfactory for closely

stiffened shells that fail in general instability, since the effect of the discreteness of stiffeners is usually negligible. The adequacy of smeared stiffener theory, is still in question and must be verified. A review of experimental work to assess the bounds and extent of applicability of linear smeared theory was given Singer (Ref 10).

In outline, the analysis employed the Donnell stability equations through the force and moment expressions. In the mathematical model, the stiffeners are smeared to form a cut layer of many parallel rings or stringers which touch each other but are not connected. The main assumptions are:

a. The stiffeners are distributed over the whole surface of the shell.

b. The normal strains vary linearly in the stiffener as well as in the skin. The normal strains in the skin and the stiffener are equal at their point of contact.

c. The inplane shear membrane force is carried entirely by the shell.

d. The torsional rigidity of the stiffener is added to that of the skin.

The analysis is outlined in (Ref 10) and given in detail in (Ref 11). The resulting equations have been solved for a variety of boundary conditions. For clamped ends a Galerkin technique was employed since the equations could not be solved directly.

The main objective of investigating linear smeared

stiffener theory is to determine the effectiveness of the stiffeners and their relative importance. Batdorf (Ref 6) has shown that the shell geometry can be characterized by a single parameter Z.

$$Z = (1-nu^2)^{\frac{1}{2}} (L^2/Rh) \qquad (10)$$

The important stiffener parameters are spacing, shape, cross sectional area, and eccentricity.

Cross sectional area is usually the most important geometric property of the stiffener determining their effectiveness. However, it also directly affects the weight and must be minimized. For an axially loaded cylindrical shell, stringers are the most efficient stiffeners. Outside stringers have been shown to be always more efficient than an equivalent weight unstiffened shell.

Rings are much less effective than stringers in the stiffening of cylindrical shells under axial load, when alone. But, when they are added to an axially stiffened shell, the buckling load is increased significantly.

As was done for unstiffened cylindrical shells, the effects of boundary conditions have been investigated for stiffened cylindrical shells. The effects for external and internal stringers are significantly different, and depend strongly on the stringer geometry. In general, the axial restraint ($u^* = 0$ instead of $N_x = 0$) is the predominant factor for simple supports. With internal stringers, axial restraint ($u^* = 0$ instead of $N_x = 0$) increases the buckling

load about 45%.

With external stringers, axial restraint is less effective, and for weaker stringers the effectiveness of axial restraint decreases even more.

For stringer stiffened shells under axial compression, rotational restraint is a major factor which raises the buckling load considerably.

The effect of non-linear prebuckling deformations were considered. Singer (Ref 10) found that non-linear prebuckling deformations apparently were not a major factor in the determination of the buckling load of stiffened cylindrical shells. However, for short stringer stiffened cylindrical shells, the non-linearity in the prebuckling deformations may warrant further study.

Another boundary effect of stringer stiffened shells is the load eccentricity. The usual analyses assume that the load is applied at the skin midsurface. The end moments caused by this eccentricity may have a significant effect on the buckling load. The length of the shell affects the magnitude of this effect. That is, for a short shell this effect is small, while for a longer shell this effect is much greater. Moments which tend to bend the shell middle outward (and give rise to tensile hoop stresses), increase the buckling load. Hence, for internal stringers, loading through the shell midsurface decreases the buckling load.

In 1962, Professor Van der Neut stated that he expected a reduction in imperfection sensitivity in stringer stiffened

shells with the conclusion that linear theory would be adequate to predict their buckling loads for general instability.

Singer indicates that stiffener area ratio is an important factor in stringer stiffened shells. It is, however, not the only important parameter in the problem; the shell geometry parameter Z is of equal importance.

Initial imperfections have been identified as the main cause of the large discrepancies between experimental and theoretical buckling loads of unstiffened cylindrical shells under axial compression. For closely stiffened shells, the influence of imperfections is less pronounced, however, imperfections remain the primary degrading factor.

Another factor recently shown to cause scatter in experimental buckling stress is the effect of inelasticity at low values of R/h. This plasticity occurs even when S_{cr} is well below the elastic limit. Hence, variation of the elastic limit of the material could cause some scatter at all values of R/h.

Singer discusses various attempts by several authors to determine the optimum structural efficiency of stringer stiffened cylindrical shells under axial compression. It is shown that the most efficient stiffening is for lighter stringers and thinner shell as opposed to thicker equivalent shell or heavy stringers. For the optimum efficiency $.3 < A_1/bh < .8$ for a stringer stiffened shell, where A_1 is the cross-sectional area of the stringer and b is the stringer spacing.

Practically all minimum weight design studies have been

based on linear theory. However, care must be taken in such studies because there are cases where an unstiffened shell is predicted to be more efficient than a slightly stiffened shell. Thus, an erroneous conclusion may be drawn from such a study if the much higher imperfection sensitivity of the unstiffened shell is not taken into account, since this could well reverse the relation of the actual buckling loads.

Palazotto (Ref 12) explored the validity of using linear bifurcation theory for the buckling analysis of stringer and ring-stringer stiffened cylindrical shells with rectangular cutouts. This analysis was performed using the STAGS (Ref 13) (Structural Analysis of General Shells) computer program. This program incorporates linear bifurcation theory, non-linear collapse analysis, discrete stiffening, and smeared stiffening theory.

The buckling loads of stringer and ring and stringer cylindrical shells were computed using both the linear bifurcation analysis and the non-linear collapse analysis capability of STAGS. When the results for both the linear and non-linear analyses compared within a few per cent, Palazotto concluded that linear bifurcation theory adequately predicts the buckling load of a stiffened cylindrical shell with cutouts. The importance of this fact is that a non-linear collapse analysis is much more expensive than a linear bifurcation analysis in terms of computer time.

A limited investigation was carried out to determine the effect of cutout reinforcement of stiffened cylindrical shells.

Purpose

It is the purpose of this thesis to determine the variation of buckling load with the location and volume of a reinforcing frame around a rectangular cutout in a stiffened cylindrical shell.

General Procedure

The buckling load of the cylinders investigated, were determined using the linear bifurcation capability of the STAGS (Structural Analysis of General Shells) computer program and smeared stiffener theory. Four parameters were varied in this study: stringer versus ring and stringer shell stiffening, cutout size, reinforcing frame to cutout volume ratio, and frame position.

II. Theory and Modeling

General Description of Stags

STAGS (Structural Analysis of General Shells) is a computer program to analyze the behavior of general shells under arbitrary static and thermal loading. Non-linearities caused by plasticity and deformations are accounted for. STAGS is based upon an energy formulation in which the derivatives are replaced by their two-dimensional finite difference approximations. Minimization of the potential energy leads to, in the general case, a non-linear set of algebraic equations which are solved by a modified Newton-Raphson technique.

STAGS can perform either elastic or plastic analyses of shells. For the elastic portion of STAGS three types of analyses may be performed; linear elastic, classical bifurcation with linear prebuckling displacements, and non-linear elastic collapse analysis. STAGS also performs a non-linear inelastic analysis, but does not permit the temperature or material properties to vary with the space coordinates.

Geometry is defined using any one of the standard shell geometry options (plate, circular, cylinder, etc.); or the user can easily write a subroutine to define his own particular geometry.

Shell stiffening can be accomplished in several ways. First, discretely located stiffeners can be positioned

anywhere on the shell surface along a coordinate line. Second, the entire shell may be stiffened by using the "smeared" stiffener capability. Lastly, a subroutine can be added to the program to define the stiffness properties of the shell wall, to which stiffener effects can be added. The user also has the option to specify one of the standard wall configurations. Provisions have been made to incorporate shell cutouts along coordinate lines.

Outline of STAGS Theory

A review of the theory used in STAGS is given below. A more complete treatment of the theory is given in (Ref 14).

The solution procedure used in STAGS is based upon the principle of stationary potential energy. The shell surface is covered with mesh lines parallel to the coordinate lines. The degrees of freedom are the displacements u, v, and w in the axial, circumferential, and radial directions, respectively.

The total strain energy of the shell is obtained by numerically integrating the strain energy density over the surface of the shell. For the integration procedure the shell surface is divided into a number of subareas, in which each subarea corresponds to the intersection of two mesh lines. The displacements and their derivatives are replaced by the appropriate finite difference approximations. A vector, Z^i, of strains and curvature changes is evaluated at mesh station i, where:

$$Z^{i^T} = \left[e_x \; e_\theta \; e_{x\theta} \; K_x \; K_\theta \; K_{x\theta}\right] \tag{11}$$

Z^{i^T} indicates the transpose of Z^i. Note that Z^i is, in general, a non-linear function of the displacements and their derivatives at mesh station i.

The displacements and derivatives at mesh station i are approximated using finite difference techniques, hence, the approximated displacements, their derivative, and Z^i are functions of the "raw" displacement unknowns surrounding mesh station i. Excellent descriptions of finite difference approximations can be found in the works by Deschler (Ref 16) and Wiley (Ref 17), therefore finite difference approximations will not be discussed further.

The total vector of raw displacement unknowns is:

$$X^T = \left[u^1 \text{ --- } u^i \; v^i \; w^i \text{ --- } w^{i_{max}}\right] \tag{12}$$

where u^i, v^i, and w^i are the "raw" displacement unknowns at mesh station i, and i_{max} is the total number of mesh stations. Note that there are $3 \cdot i_{max}$ displacement unknowns.

The strain energy density at mesh station i, ΔU^i, is a function of the strains and curvature changes. Let the matrix D^i at station i be defined as:

$$D^i_{kl} = {}^{\Delta}U,^i_{kl} \tag{13}$$

where a subscript following a comma indicates differentiation with respect to one of the strains or changes of curvature. For k = 1,2,3,4,5,6, the derivatives are to be taken with respect to e_x, e_θ, $e_{x\theta}$, K_x, K_θ, $K_{x\theta}$, respectively.

A derivation of D^i for a shell with smeared stringers is given in (Ref 13). The strain energy density at subarea a^i is:

$$\Delta U^i = Z^{i^T} D^i Z^i \tag{14}$$

ΔU^i is a fourth degree polynomial in the displacement unknowns. Summing strain energy contributions for all subareas yields the total strain energy for the shell.

$$U = \sum_i {}^{\Delta} U^i a^i \tag{15}$$

If F is the vector of external forces corresponding to the displacement unknowns, then the potential energy of the work done by external forces, W, can be expressed as

$$W = X^T F \tag{16}$$

The total potential energy of the system is:

$$V = U-W \tag{17}$$

Note that the potential energy, V, is a fourth degree polynomial in the displacement unknowns. Static equilibrium requires that the first variation of the potential energy be equal to zero and leads to the equation:

$$LX = F \tag{18}$$

where the non-linear "stiffness" operator for the displacement unknowns is defined by the following equation:

$$LX = \text{grad } U \tag{19}$$

or equivalently the rows, $[LX]_i$, of LX are defined as:

$$[LX]_i = \frac{\partial U}{\partial X(i)} \tag{20}$$

where X(i) is the i^{th} component of the vector of displacement unknowns.

When only linear terms are included in the strain and curvature change relations, L degenerates into a linear operator of matrix form.

When L is non-linear, iterative techniques must be employed for the solution of Eq. (18). A general collapse analysis requires that Eq. (18) be solved for a sequence of applied loads. A reasonably good initial approximation of the solution and a series of moderately increasing load steps are required for reliable detection of collapse due to the non-uniqueness of the solutions to non-linear equations. The requirement that Eq. (18) be solved repeatedly using iterative techniques, is what makes a non-linear collapse analysis so expensive compared to a linear bifurcation analysis (described later).

A brief description will be given of a modified Newton-Raphson method used in the solution of Eq. (18) for the displacement unknowns, X. For a function g(x) = 0, the well-known Newton-Raphson iteration is:

$$X_{i+1} = X_i - g(X_i)/g'(X_i) \tag{21}$$

where X_i is an approximate solution to g(x) = 0 and X_{i+1} is a better approximation. Repeated application of Eq. (21)

yields a solution to $g(x) = 0$ to any desired accuracy. Notation will be simplified with introduction of:

$$L'_{ij} = \frac{\partial^2 U}{\partial X(i) \partial X(j)} \tag{22}$$

Unless the non-linear terms of L are dropped, L' will be a function of a particular displacement vector X_k, and will be designated L'_{X_k}. With L'_{X_k} the Newton-Raphson method can be readily extended to solve Eq. (18). The iteration is:

$$X_{k+1} = X_k + L'^{-1}_{X_k} (F - L_{X_k}) \tag{23}$$

$L'^{-1}_{X_k}$ indicates the inverse of L'_{X_k}. The inversion requires that L'_{X_k} be non-singular, that is, a unique solution of Eq. (18) requires that the determinant of L'_{X_k} be non-zero.

The most effective use of Eq. (23) in the solution of Eq. (18) suggests only periodic recomputation and inversion of L'_{X_k}, since the computer execution time required to invert L'_{X_k} is high compared to the time required to evaluate the reaminder of Eq. (23). The modified form of the Newton-Raphson method used in STAGS is:

$$X_{k+1} = X_k + L'^{-1}_{X_m} (F - LX_k) \tag{24}$$

where the subscript m indicates the last iteration for which $L'^{-1}_{X_m}$ was recomputed.

The mathematical characterization of bifurcation buckling is provided by the generalized Newton-Raphson method. Let X satisfy Eq. (18) under the load vector F, then if for

every neighborhood of X there exists another vector Y such that

$$L_X Y = F \tag{25}$$

then bifurcation buckling has occurred at load F. As previously mentioned, a unique solution of Eq. (18) using the iteration scheme of Eq. (23) requires that L'_{X_k} be non-singular. Conversely, if there are multiple solutions of Eq. (18) then L'_{X_k} is singular, in which case:

$$\det (L'_{X_k}) = 0 \tag{26}$$

Let:

$$X = \lambda X_L \tag{27}$$

where X_L is the vector of displacement unknowns that satisfies Eq. (18) for a given load vector F_L. Substituting Eq. (27) into equation (26) we obtain:

$$\det (L'_{\lambda X_L}) = 0 \tag{28}$$

For classical buckling in which prebuckling rotations are ignored, only the linear terms of $L'_{\lambda X_L}$ are retained, resulting in an eigenvalue problem of the form:

$$\det (A-\lambda B) = 0 \tag{29}$$

The specific method employed to obtain the fundamental eigenvalue λ and its eigenvector is not mentioned in the STAGS manuals (Ref 13) and (Ref 14). If the reader wishes more information in this area, a description of the Power

Method can be found in (Ref 18) and several methods as applied to a large finite-element program are described in the NASTRAN Theoretical Manual (Ref 19). The buckling load vector F_{cr} is a multiple of the applied load vector for the linear solution.

$$F_{cr} = \lambda F_L \tag{30}$$

The formation of the A and B matrices in Eq. (29) will be considered briefly. From Eq. (15) we know that:

$$\frac{\partial^2 U}{\partial X(i)\partial X(j)} = \sum_k a^k \frac{\partial^2 \Delta U^k}{\partial X(i)\partial X(j)} \tag{31}$$

Using Eq. (14) the k^{th} term of Eq. (31) is:

$$\frac{\partial^2 \Delta U^k}{\partial X(i)\partial X(j)} = \frac{\partial Z^{k^T}}{\partial X(i)} D^k \frac{\partial Z^k}{\partial X(j)} + \frac{\partial^2 Z^{k^T}}{\partial X(i)\partial X(j)} \lambda S_L^k \tag{32}$$

where S_L^k is the linear stress resultant vector at mesh station k. The more general (non-linear) stress resultant vector is:

$$S^k = D^k Z^k \tag{33}$$

where

$$S^{k^T} = \lfloor N_x \; N_\theta \; N_{x\theta} \; M_x \; M_\theta \; M_{x\theta} \rfloor \tag{34}$$

The terms generated by the first term on the right side of Eq. (32) make up the A matrix, and represent contributions from membrane energy.

The second term in Eq. (32) contributes to the B matrix and represents the bending energy.

An example of the derivation of the constitutive relations, Eq. (33), for a shell with smeared stringers is given in (Ref 13).

Modeling

The shells investigated in this thesis were stiffened circular cylindrical shells with reinforcements around two symmetrically placed rectangular cutouts. The linear bifurcation capability of STAGS was used to predict buckling loads, as opposed to a non-linear collapse analysis which would have required considerably more computer time. The accuracy of linear bifurcation theory for stiffened cylindrical shells using STAGS was substantiated by Palazotto in (Ref 12). He analyzed a stringer stiffened shell with two rectangular cutouts. The finite difference mesh consisted of 602 mesh points, with a concentration of mesh points in the vicinity of the cutouts. Due to triple symmetry only one-eighth of the shell was analyzed.

The buckling load for this shell was computed using both linear bifurcation theory and non-linear collapse theory. Despite the fact that the radial displacements were considerably greater for the non-linear analysis, the buckling load predicted by linear bifurcation theory was only 6.87 per cent higher than the collapse load predicted by non-linear theory. This is an acceptable level of accuracy since the expense of non-linear analyses would severely limit the affordable range of parameters that could be

investigated.

Smeared stiffener theory was used to represent the uniformly spaced rings and stringers stiffening the entire shell. An alternate method was to specify a discrete stiffener for ring or stringer. The additional input time required for discrete stiffening was not justified by a commensurate increase in accuracy of the buckling load as shown by Palazotto (Ref 12). He indicated that the difference in buckling loads using smeared stiffeners and discrete stiffeners amounted to less than four percent for a similar problem.

On the basis of the number of mesh points used by Palazotto and current geometry, the author used a minimum of 776 mesh points.

The reinforcing frame around the cutout was modeled using discretely located stiffeners.

III. Results

Model Description

In this thesis, a stiffened circular cylindrical shell with a reinforcing frame around the cutout was analyzed for a variety of parameters. The basic geometry was held constant while four parameters were varied independently:

Internal Stiffening

- Stringers Only
- Rings and Stringers

Total Cutout Size 2a

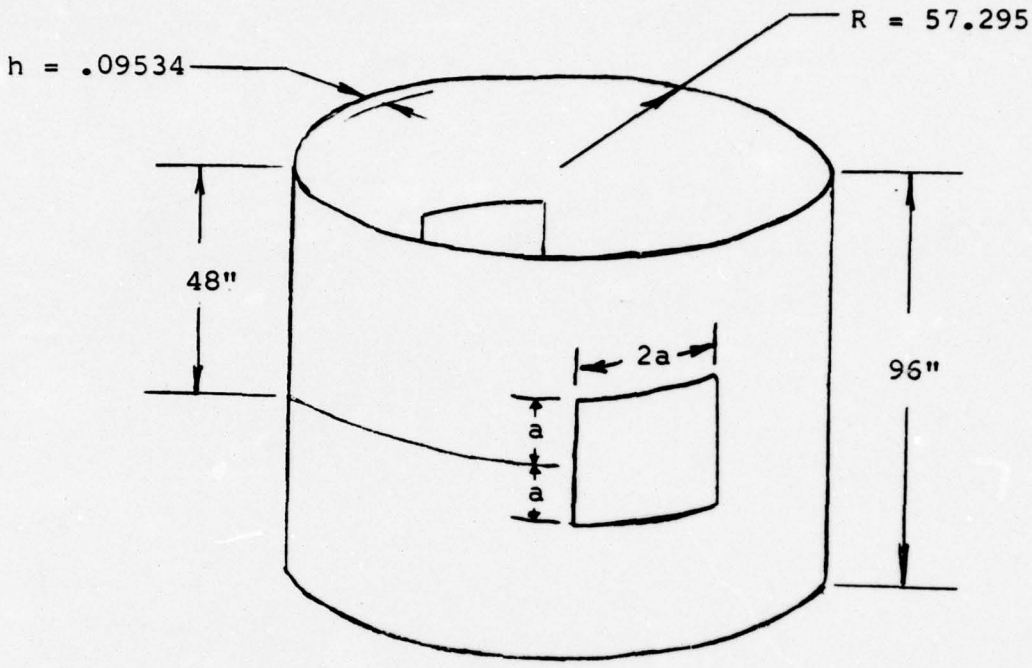
- 12 x 12 in. total cutout size
- 24 x 24 in. total cutout size

Ratio of reinforcing frame volume to removed cutout volume

- $W_{sf}/W_o = 0.5$
- $W_{sf}/W_o = 1.0$
- $W_{sf}/W_o = 1.5$
- $W_{sf}/W_o = 2.0$

Reinforcing frame position (4 positions)

The basic shell geometry is shown in Fig. 3. The



Cutout Sizes

2a = 12"

2a = 24"

E = 10^7psi

nu = .333

G = $3.75 \cdot 10^6$psi

Z = 1591.



Portion of Shell Analyzed

Figure 3. Basic Shell Geometry

radius of the shell was chosen such that the circumferential coordinate was numerically equal in either degrees or inches. The length was chosen such that a finite difference mesh could be imposed upon the shell compatible with the stiffener and reinforcing frame locations and the cutout boundaries, since STAGS requires that the discrete stiffeners and the cutout edges lie along mesh lines. Smeared stiffeners should also lie along mesh lines for accurate representation. The value of Z for this shell is 1591. The overall dimensions were chosen so that this thesis could be compared with previous work by Palazotto (Ref 12). The dimensions given, approximate a large missle interstage.

The smeared stiffener geometry and spacing are indicated in Fig. 4. The ring and stringer geometries were decided upon in order to approximate those that would be expected in actual applications. The two to one ratio of the height to width was chosen as compromise of good bending stiffness and yet reasonable torsional stiffness.

The two cutout sizes used were a = 6" and a = 12" corresponding to 12" x 12" and 24" x 24" cutouts respectively. The value of the cutout size parameter, $a/(Rh)^{\frac{1}{2}}$, is 2.57 and 5.13 for a = 6" and a = 12", respectively. The value of a = 12 approximated the largest cutout size for which linear theory is valid (Ref 12).

The reinforcing frame volume to removed cutout volume ratios correspond to the situation where the reinforcing frame weighs from one-half to twice the weight of the

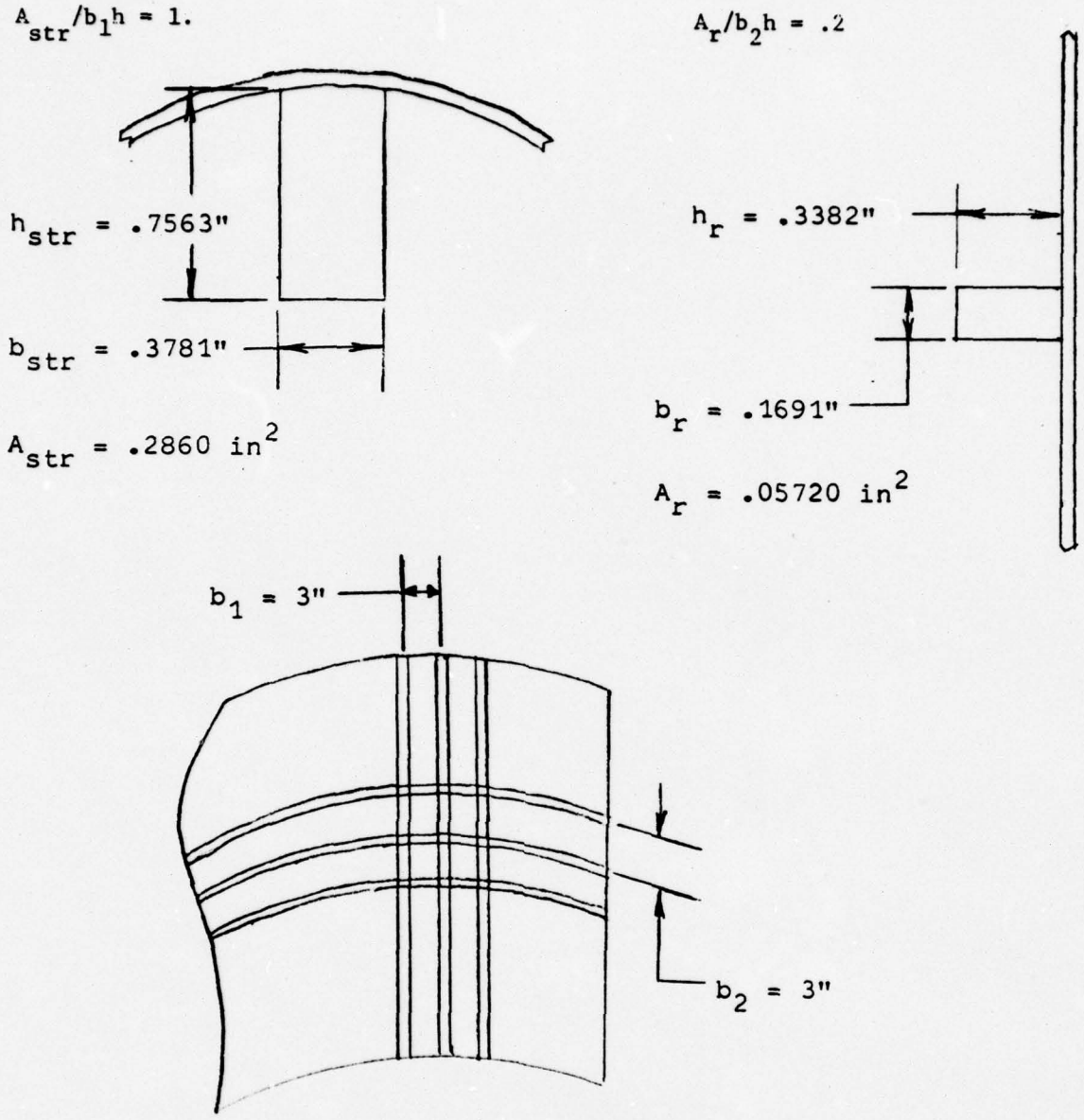


Figure 4. Smeared Stiffener Geometry and Spacing

material removed for the cutout. This was considered as large a range as would be of practical interest.

Note that the frame positions shown in Fig. 5 are different for a = 6" and a = 12". The maximum frame positions were chosen as being the maximum distance at which the frame would have a significant impact on the buckling load as determined in (Ref 12).

Note that for a given volume ratio the total frame volume remained constant as the frame position was varied. This was necessary in order to validly compare the most efficient frame position for a given volume ratio.

The equations for the geometric properties of the reinforcing frame will be discussed. The volume per unit area of the cutout for the stringer stiffened shell is WOA = .19068 IN^3/IN^2; and for the ring and stringer stiffened shell WOA =.20975 IN^3/IN^2. The cross sectional area of stiffening frame is given by:

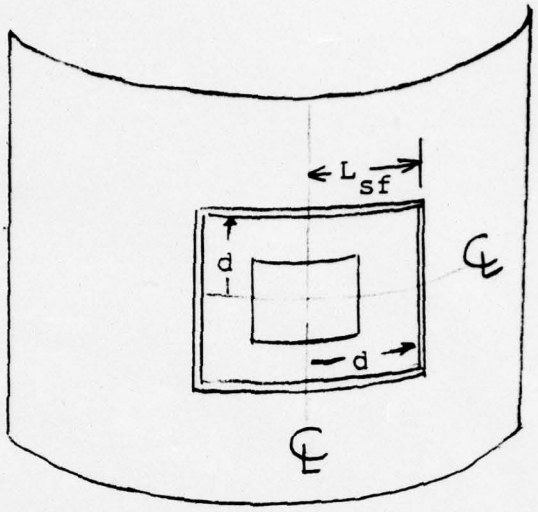
$$A_{sf} = a^2 WOA\ (W_{sf}/W_o)/2d \tag{35}$$

where 2a is the total cutout dimension and d is the distance from the cutout centerline to the stiffening frame. For a square cross-section, the height and width of the stiffening frame become:

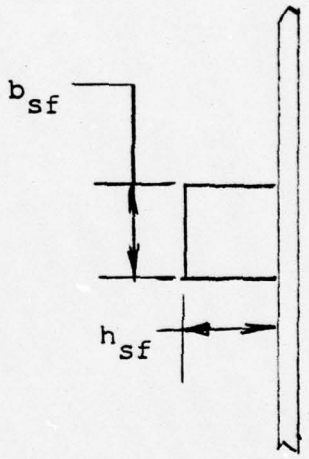
$$b_{sf} = h_{sf} = (A_{sf})^{\frac{1}{2}} \tag{36}$$

The moments of inertia equal:

$$I_{x \text{ or } y} = I_z = b_{sf} h_{sf}^3/12 = h_{sf}^4/12 \tag{37}$$



Note: Frame volume remains constant for a given volume ratio W_{sf}/W_o



POSITION	2a = 12"	2a = 24"
1	6.0	12.0
2	7.5	13.5
3	9.0	15.0
4	12.0	18.0
5	15.0	
6	18.0	

Frame distance, d, from the centerline of the cutout

Figure 5. Reinforcing Frame Locations

The torsional stiffness constant (Ref 15), for b/h = 1 is

$$J_{sf} = .1406\ b_{sf}^3\ h_{sf} \tag{38}$$

For the present value of G

$$GJ_{sf} = 527382.\ h_{sf}^4 \text{ psi} \tag{39}$$

The values of the frame properties described above are given in Appendix A. The listing is ordered according to computer run number with the geometric parameters shown for each run.

The analysis was carried out over one-eighth of the shell surface since the loading and shell were triply symmetric about the planes x = 48", $\theta = 0^\circ$, and z = 0". Sufficient accuracy with the minimum number of mesh points, required separate finite difference mesh arrangements for a = 6" and a = 12". These meshes are shown in Fig. 6.

A uniform axial displacement was applied at the end of the cylinder. This type of loading used is comparable to usual experimental load application (Ref 9). Symmetric boundary conditions were dictated by analyzing the problem over one-eighth of the shell. The boundary conditions and enforced displacements are shown in Fig. 7.

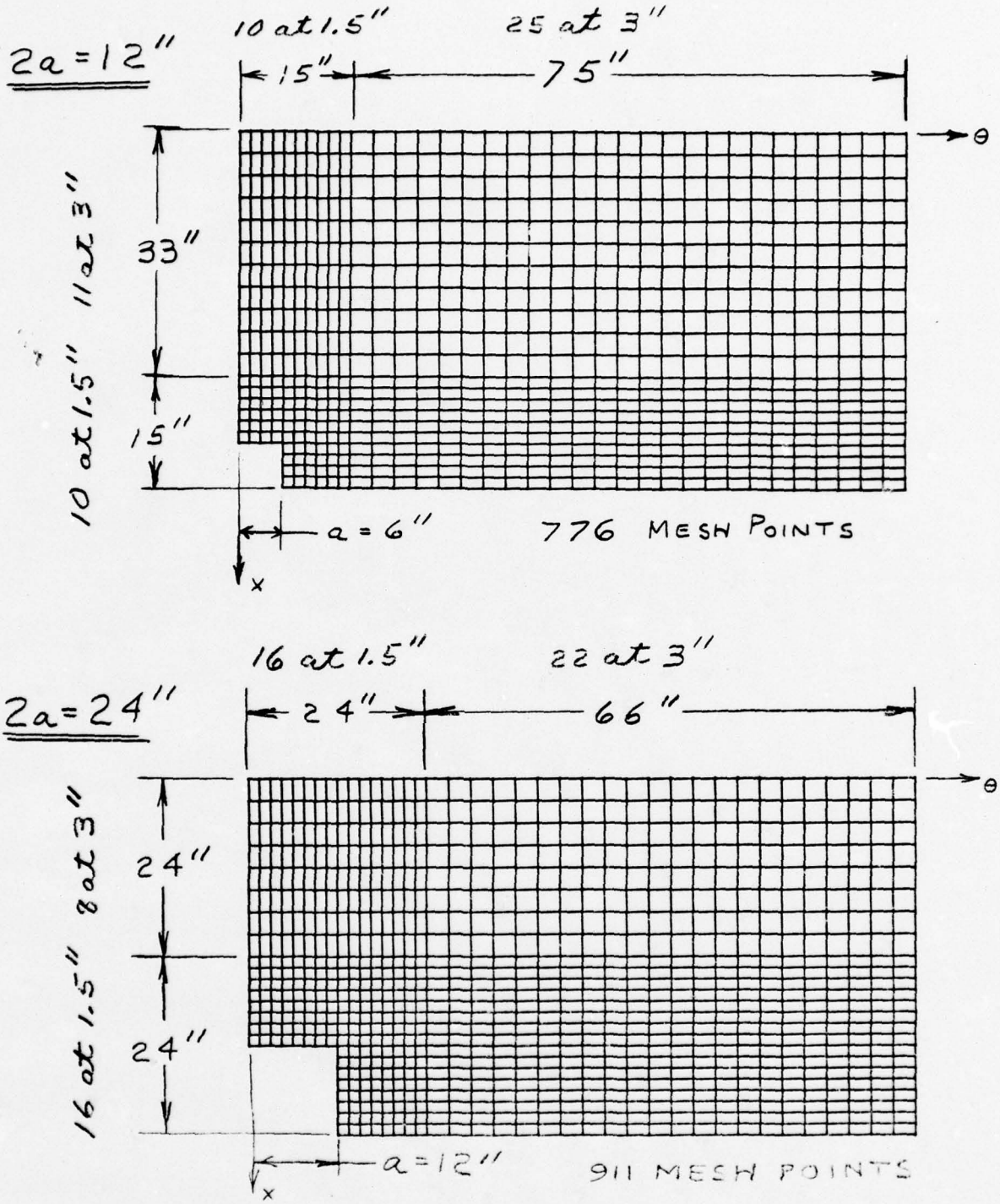
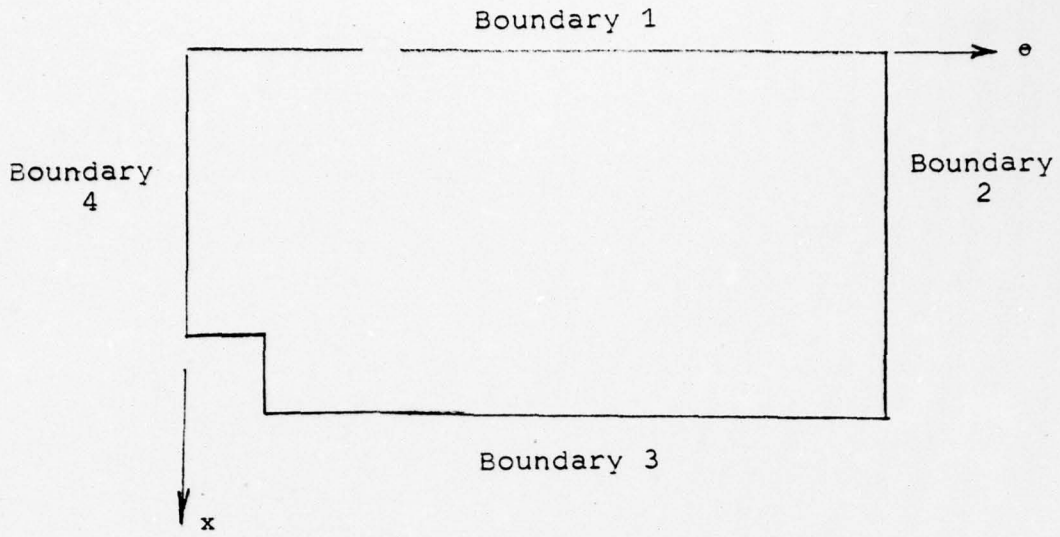


Figure 6. Finite Difference Meshes



EDGE	PREBUCKLING	BUCKLING
1	$v=w,_x=0$, $u=.1"$	$v=u=w,_x=0$
2	$v=w,_\theta=0$	$v=w,_\theta=0$
3	$u=w,_x=0$	$u=w,_x=0$
4	$v=w,_\theta=0$	$v=w,_\theta=0$

Figure 7. Boundary Conditions

Numerical Results

As previously stated, a stiffened cylindrical shell with a reinforcing frame around a cutout was analyzed for a variety of parameters using the linear bifurcation portion of STAGS.

A tabular listing of the buckling loads, P_{cr}, is given in Appendix B, according to computer run number. In addition, the ratios P_{cr}/P_o and P_{cr}/P_1 are listed, where P_o and P_1 are dependent upon the particular shell in question. P_o is the buckling load of a shell with the same type of overall shell stiffening (stringers only or rings and stringers) as the shell in question, but one that does not have cutouts or reinforcing frames. P_1 is the buckling load of a shell as described above, but with a cutout.

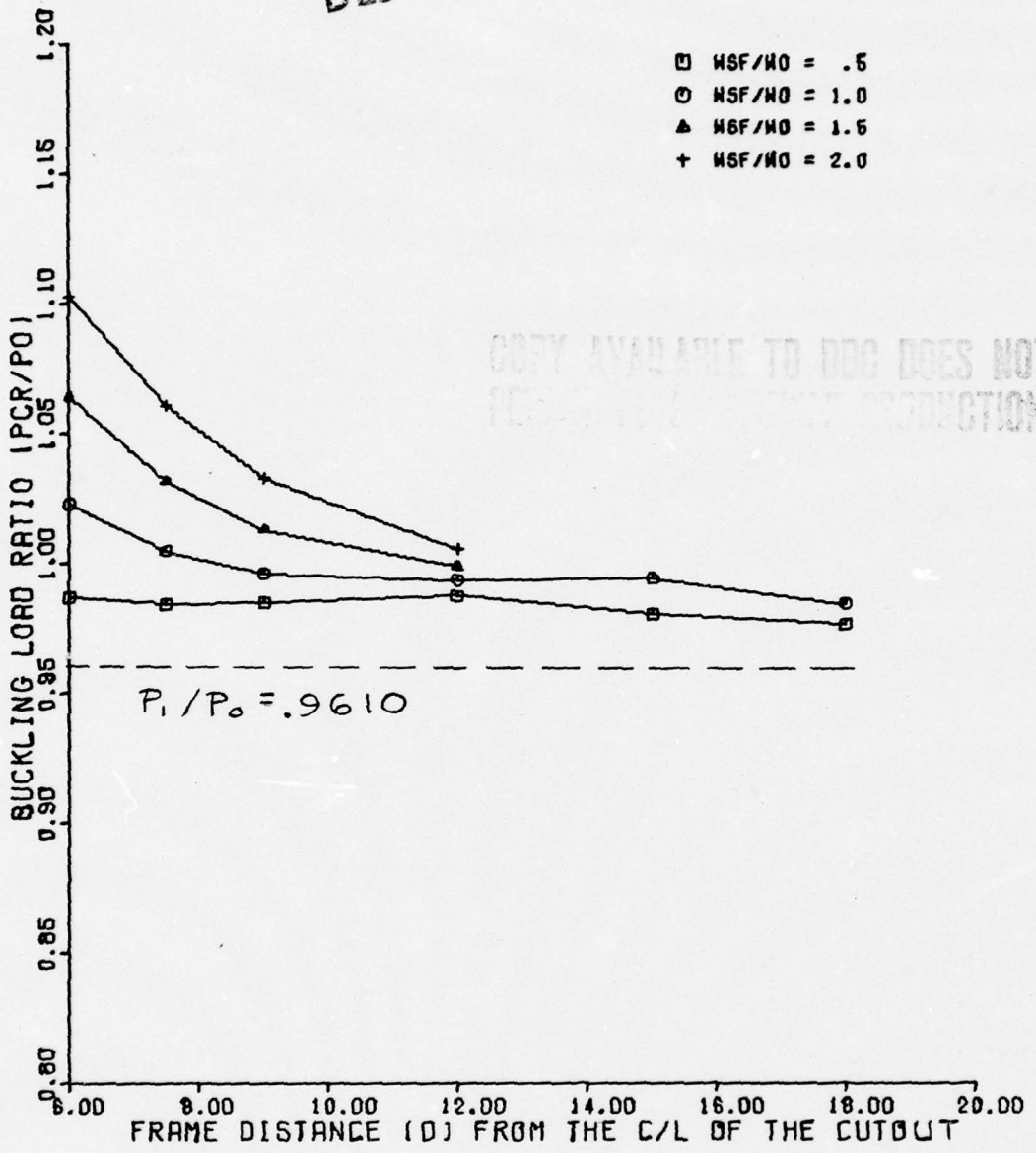
The buckling load ratio P_{cr}/P_o is plotted versus the distance, d, of the frame from the centerline of the cutout in Figures 8 through 11. Figures 8 and 9 are for stringer stiffened shells; and Figures 10 and 11 are for shells stiffened by rings and stringers. For Figures 8 and 10 the cutout size is 2a = 12"; and for Figures 9 and 10, 2a = 24". P_1/P_o has been shown for reference.

An inspection of Figures 8 through 11 indicates that the most effective position for the reinforcing frame is always along the cutout edge.

It has been observed in (Ref 12) that the general collapse shape in the vicinity of a cutout is similar to that of a shell's displacement field under a linear prebuckling analysis. Thus, it is possible to appreciate the ideal frame position by comparing the linear displacement fields of shells with

BEST AVAILABLE COPY

BEST AVAILABLE COPY



COPY AVAILABLE TO DDC DOES NOT PERMIT FULLY LEGIBLE REPRODUCTION

Figure 8. P_{cr}/P_o vs d For a Stringer Stiffened Shell, 2a = 12"

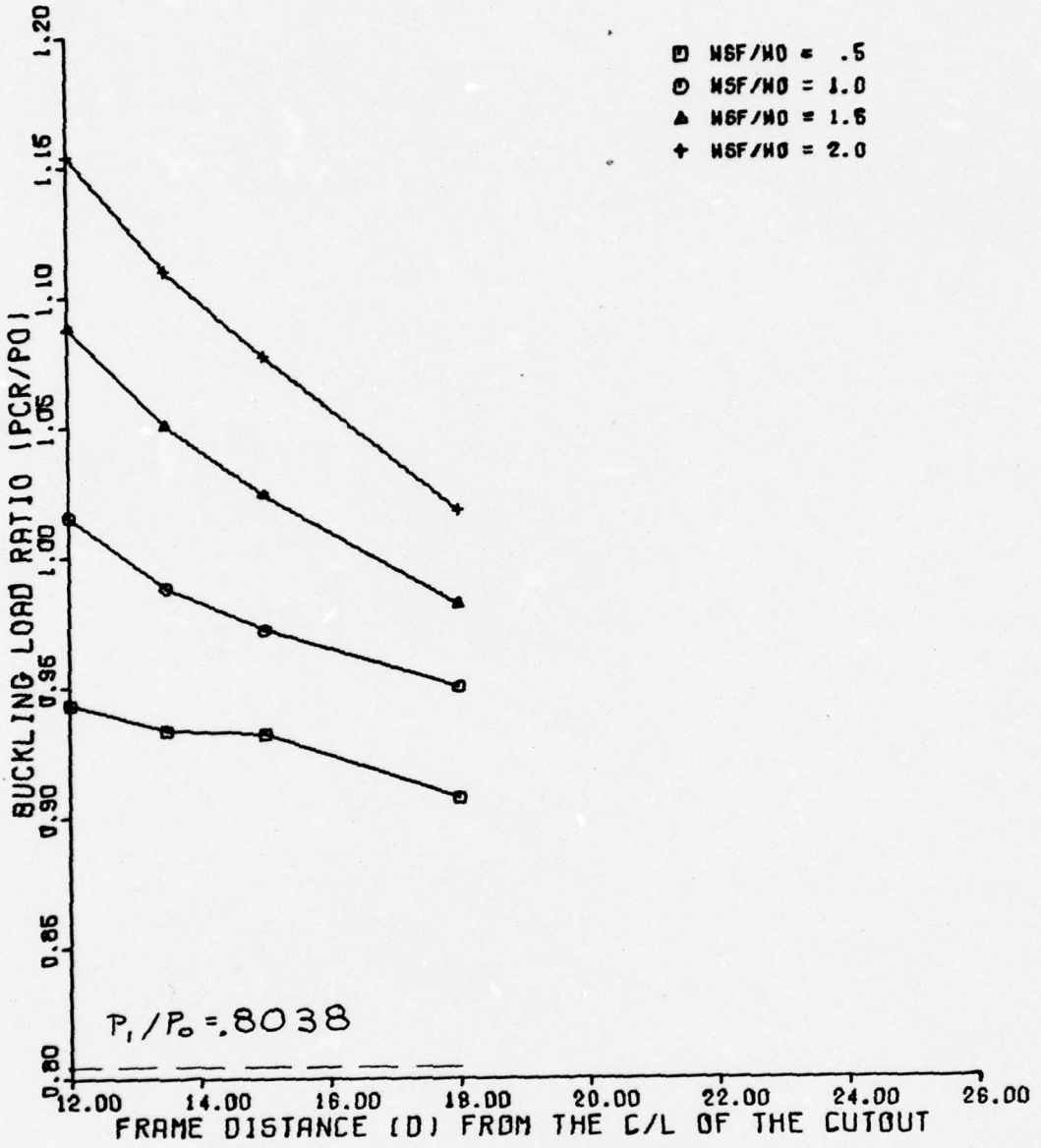


Figure 9. P_{cr}/P_o vs d For a Stringer Stiffened Shell, 2a = 24"

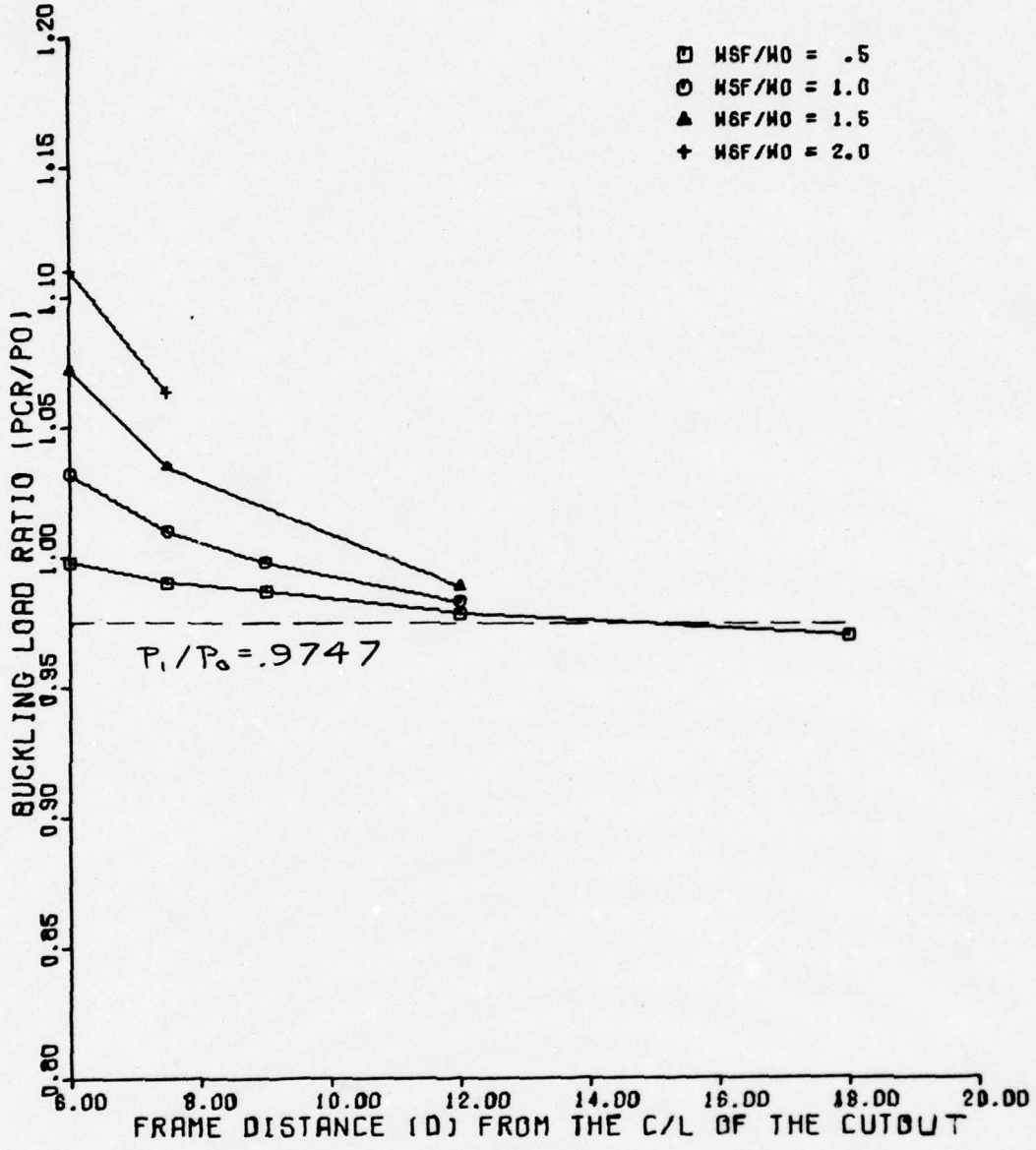


Figure 10. P_{cr}/P_o vs d For a Ring and Stringer Stiffened Shell, 2a = 12"

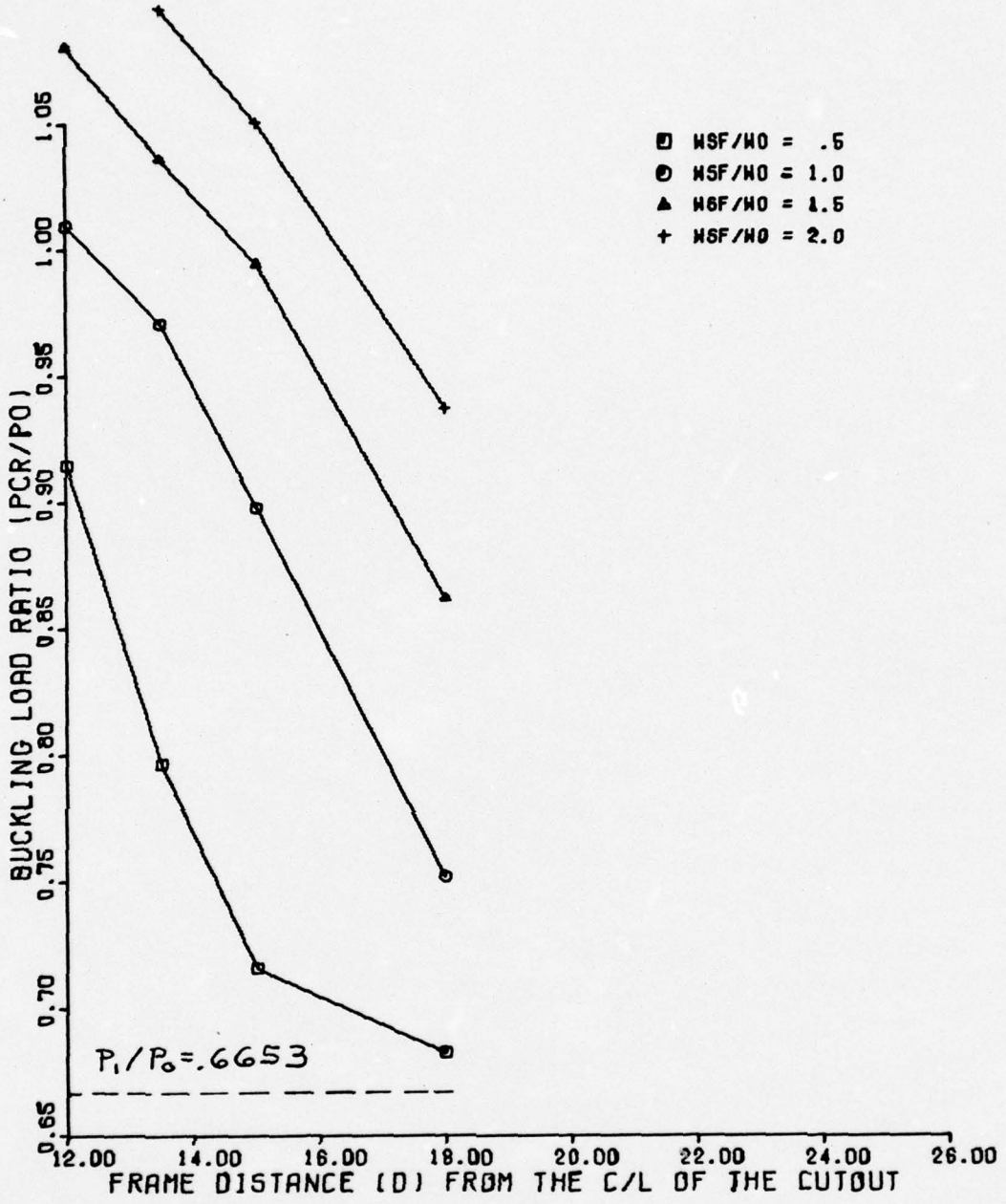
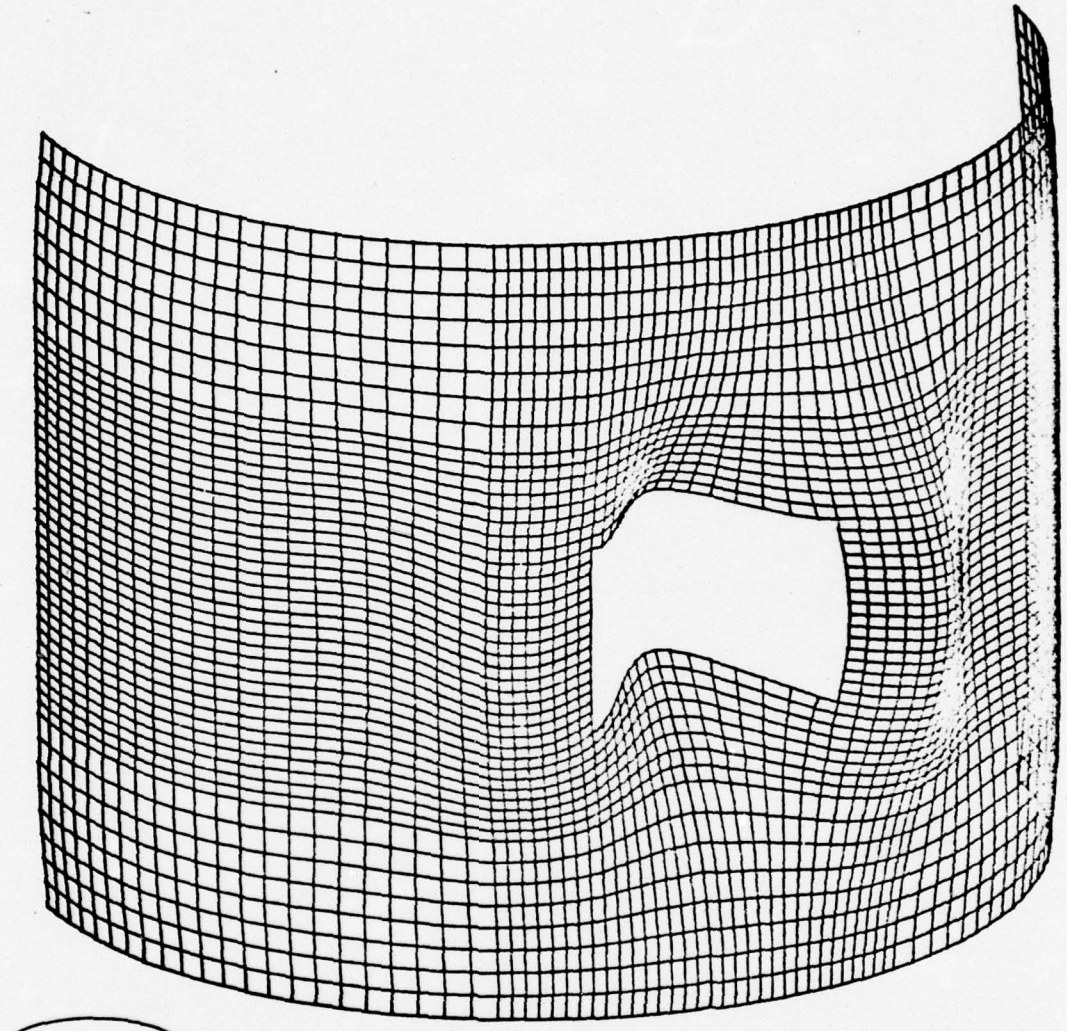


Figure 11. P_{cr}/P_o vs d For a Ring and Stringer Stiffened Shell, 2a = 24"

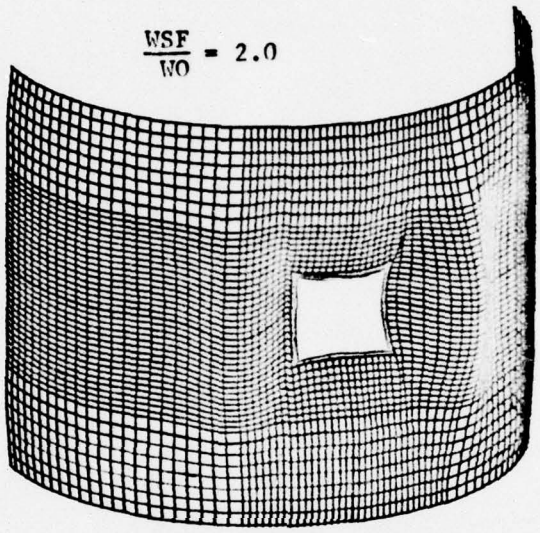
the reinforcing frames in various locations. The linear displacements of a stringer stiffened shell with a cutout size 2a = 24" and volume ratio $W_{sf}/W_o = 2$, are shown in Figures 12 and 13 for the case with no frame and the case with a frame at the cutout edge, respectively. In Figure 12, notice the large radial displacements along the upper and lower edges of the cutout. In Figure 13 the very definite stiffening effect of the frame along the cutout edge is readily apparent. Both the large radial displacements along horizontal edges and the large rotations along the vertical edges of the cutout have been dramatically reduced by the reinforcement.

An additional optimum position occurs for a stringer stiffened shell with cutout size 2a = 12" and volume ratio $W_{sf}/W_o = .5$, in which the reinforcing frame is equally effective 6" away from the cutout as it is along the cutout edge. This is in spite of the fact that at the outer position the cross-sectional area of the reinforcing frame is only half the area of inner frame (frame volume is independent of position), and the moments of inertia have a ratio of 1:4. The linear displacement fields are shown in Figures 14, 15 and 16 for no frame, a frame along the cutout edge, and a frame 6" from the cutout edge, respectively. Inspection of Figures 14 and 15 reveals that the displacements and rotations along the cutout edge are again somewhat smaller for the frame adjacent to the cutout edge than those for the unreinforced shell. For the frame 6" away



Shell Orientation in the
Displacement Plots

Figure 12. Linear Displacements For a Stringer Stiffened Shell, 2a = 24"



RUN 29 LINEAR X 25.

Note: The frame position is indicated in this and subsequent diagrams by a heavy black line

Figure 13. Linear Displacements For Run 29

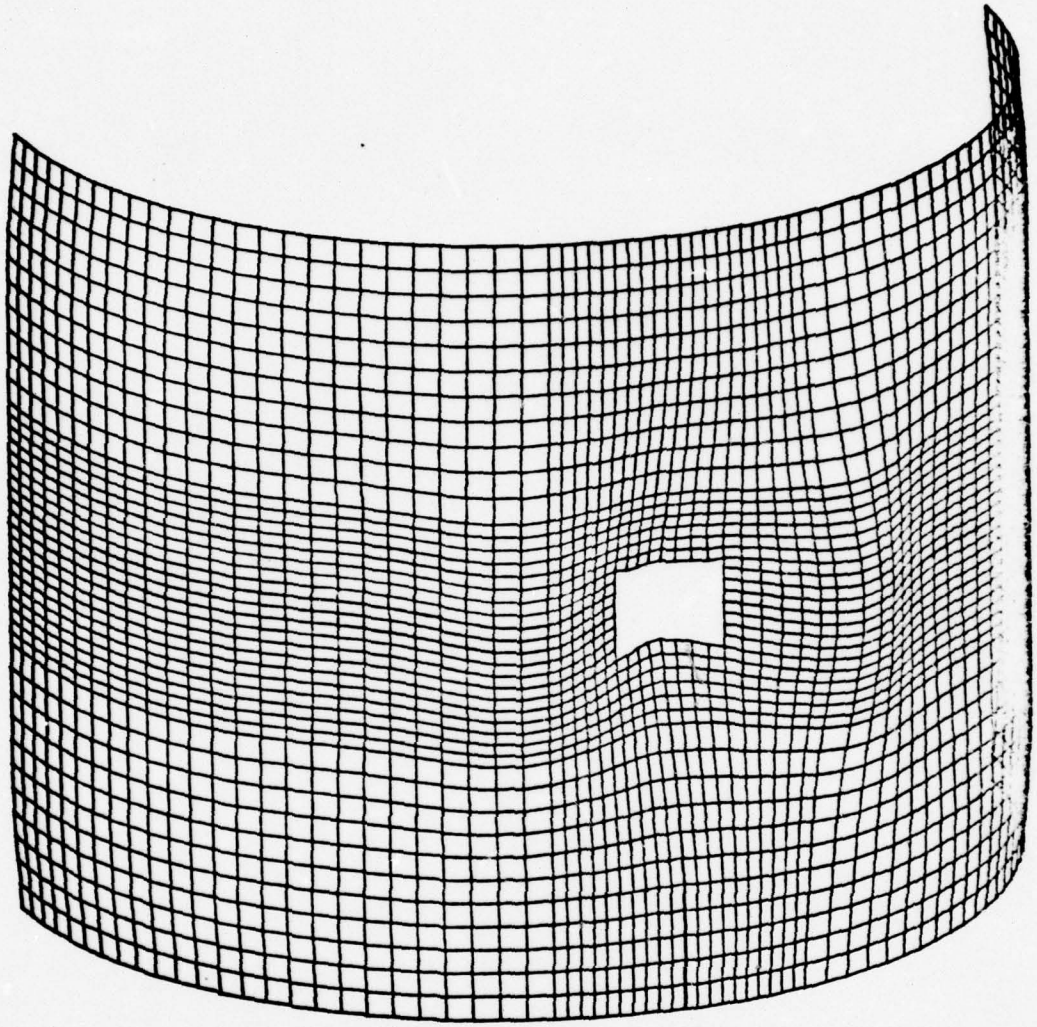


Figure 14. Linear Displacements For a Stringer Stiffened Shell, 2a = 12"

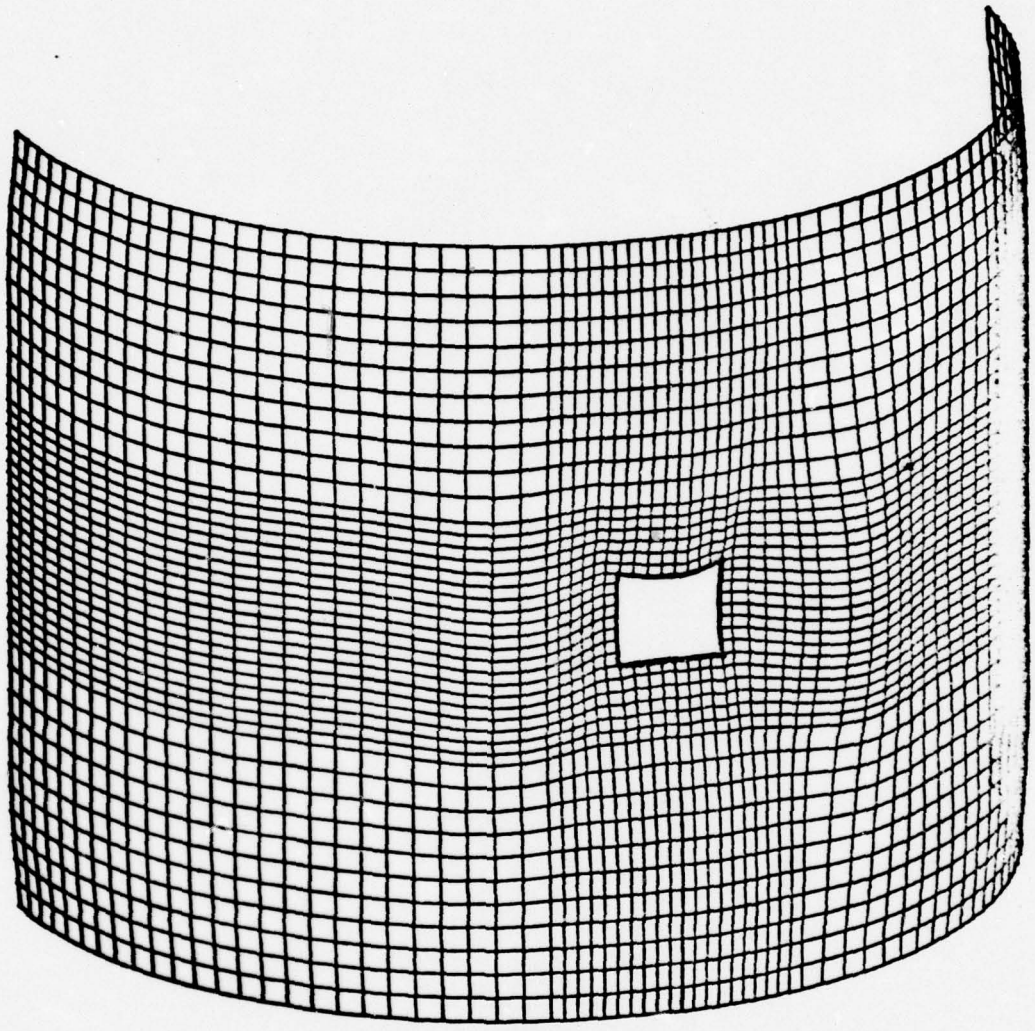


Figure 15. Linear Displacements For Run 1

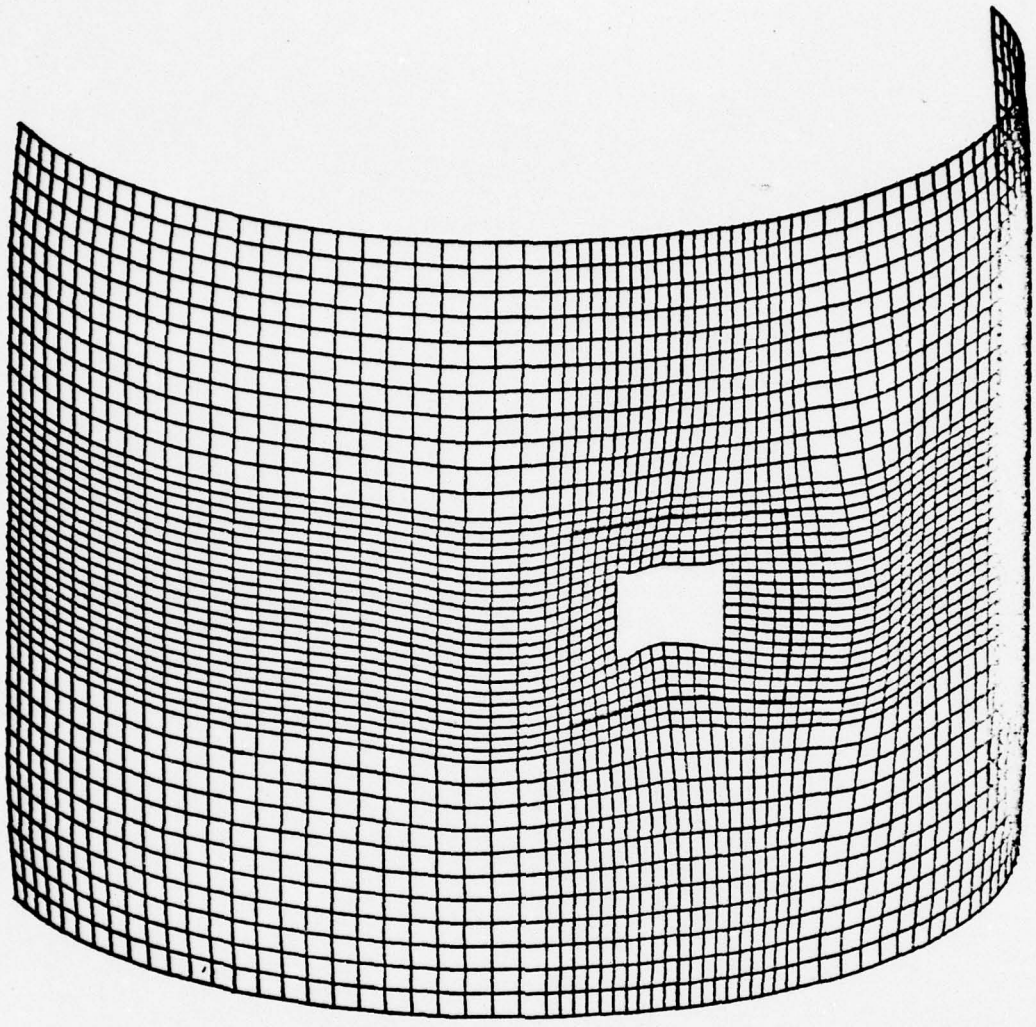


Figure 16. Linear Displacements For Run 4

from the cutout, however, the displacements are not reduced as much. Figures 17 through 19 display the axial compressive stress as a surface for the shells mentioned above. It is evident that a reinforcing frame in position 1 significantly reduces the stresses in the vicinity of a cutout below those for an unreinforced shell. This stress reduction lessens the chance for local buckling, consequently, leading to a higher shell buckling load. However, even a close examination of Figures 17 and 19, shows that a frame at position 4 yields only a slight reduction of stress in the area of the cutout.

Next, a comparison will be made of the normalized displacements (maximum displacement = 1) occurring at bifurcation; these are given in Figures 20 through 22. Comparing these Figures shows that the buckling displacements near the cutout are quite different for the reinforced and unreinforced shells. Apparently, even the small frame at position 4 is sufficient to alter the buckling mode.

The trends of the curves in Figures 8 through 11 indicate that a reinforcing frame positioned far away from the cutout may cause the shell to buckle at a load lower than the buckling load for an unreinforced shell. This, in fact, occurs in Figure 10 for a ring and stringer stiffened shell for a volume ratio $W_{sf}/W_o = .5$ with frame at position 6.

In order to suggest an explanation for this occurrance, consider a stringer stiffened shell, with $2a = 12"$, $W_{sf}/W_o = .5$, and a frame at position 6. The plots of linear prebuckling deflections and stresses are nearly identical to those for a shell without the reinforcing frame.

from the cutout, however, the displacements are not reduced as much. Figures 17 through 19 display the axial compressive stress as a surface for the shells mentioned above. It is evident that a reinforcing frame in position 1 significantly reduces the stresses in the vicinity of a cutout below those for an unreinforced shell. This stress reduction lessens the chance for local buckling, consequently, leading to a higher shell buckling load. However, even a close examination of Figures 17 and 19, shows that a frame at position 4 yields only a slight reduction of stress in the area of the cutout.

Next, a comparison will be made of the normalized displacements occurring at bifurcation; these are given in Figures 20 through 22. Comparing these Figures shows that the buckling displacements near the cutout are quite different for the reinforced and unreinforced shells. Apparently, even the small frame at position 4 is sufficient to alter the buckling mode.

The trends of the curves in Figures 8 through 11 indicate that a reinforcing frame positioned far away from the cutout may cause the shell to buckle at a load lower than the buckling load for an unreinforced shell. This, in fact, occurs in Figure 9 for a ring and stringer sitffened shell for a volume ratio $W_{sf}/W_o = .5$ with frame at position 6.

In order to suggest an explanation for this occurrance, consider a stringer stiffened shell, with $2a = 12"$, $W_{sf}/W_o = .5$, and a frame at position 6. The plots of linear prebuckling deflections and stresses are nearly identical to those for a shell without the reinforcing frame.

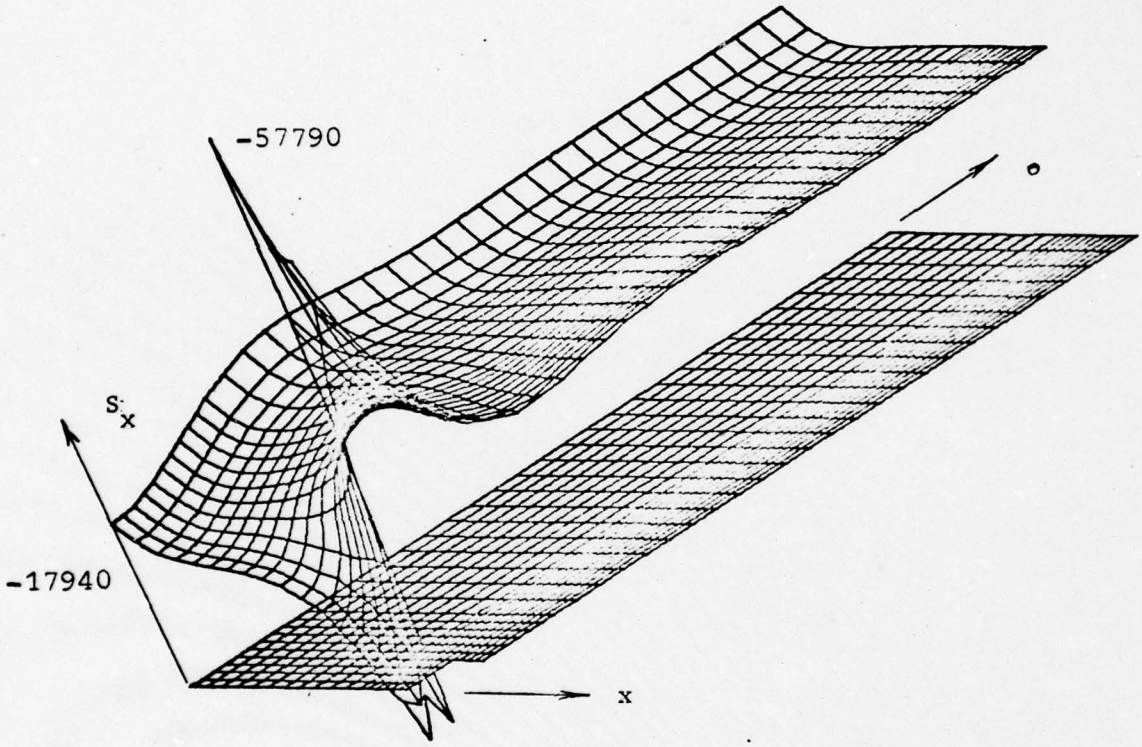


Figure 17. S_x For a Stringer Stiffened Shell 2a = 12"

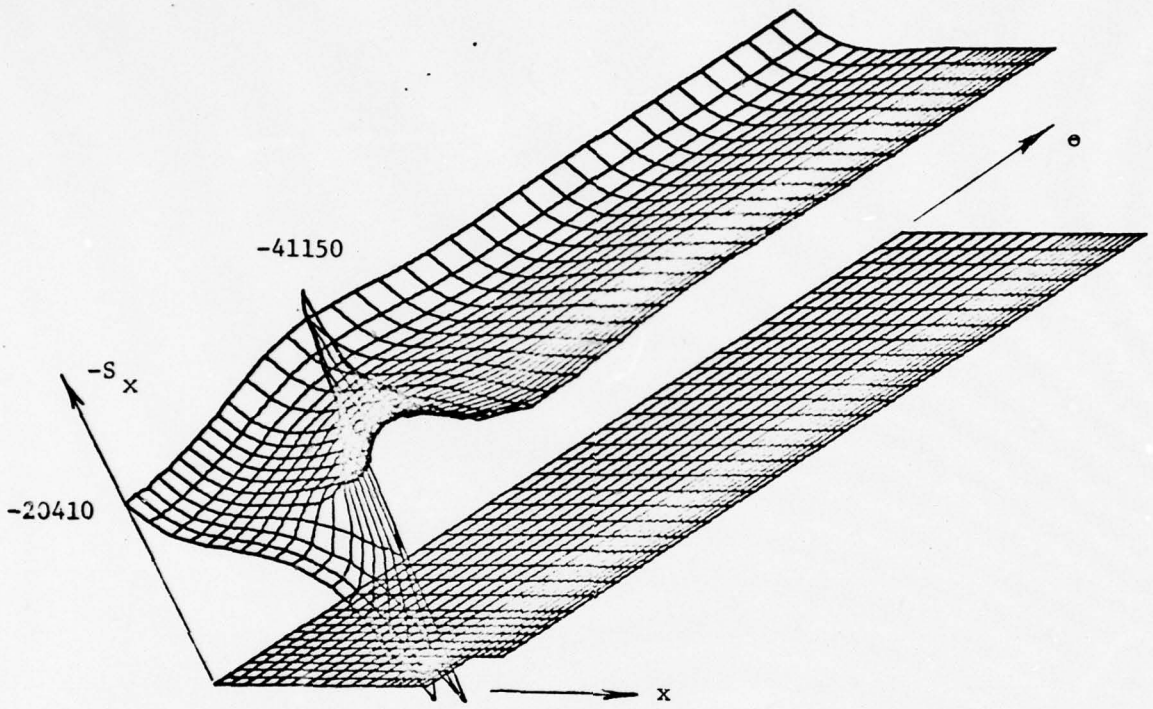


Figure 18. S_x For Run 1

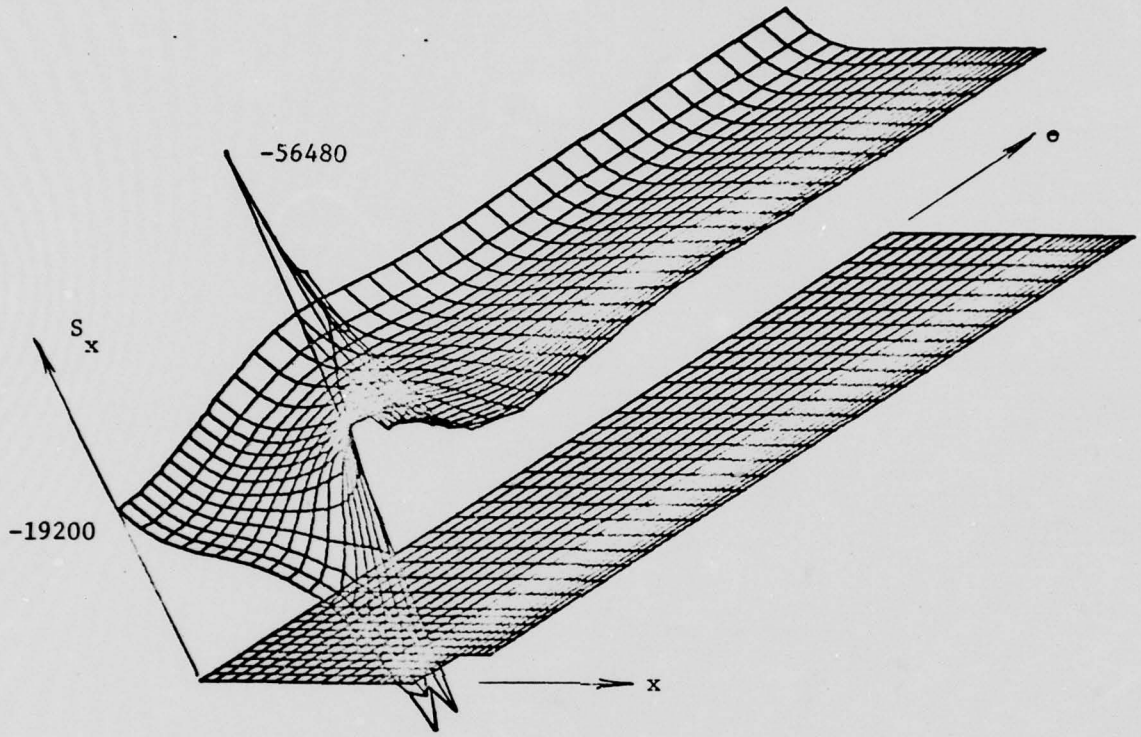


Figure 19. S_x For Run 4

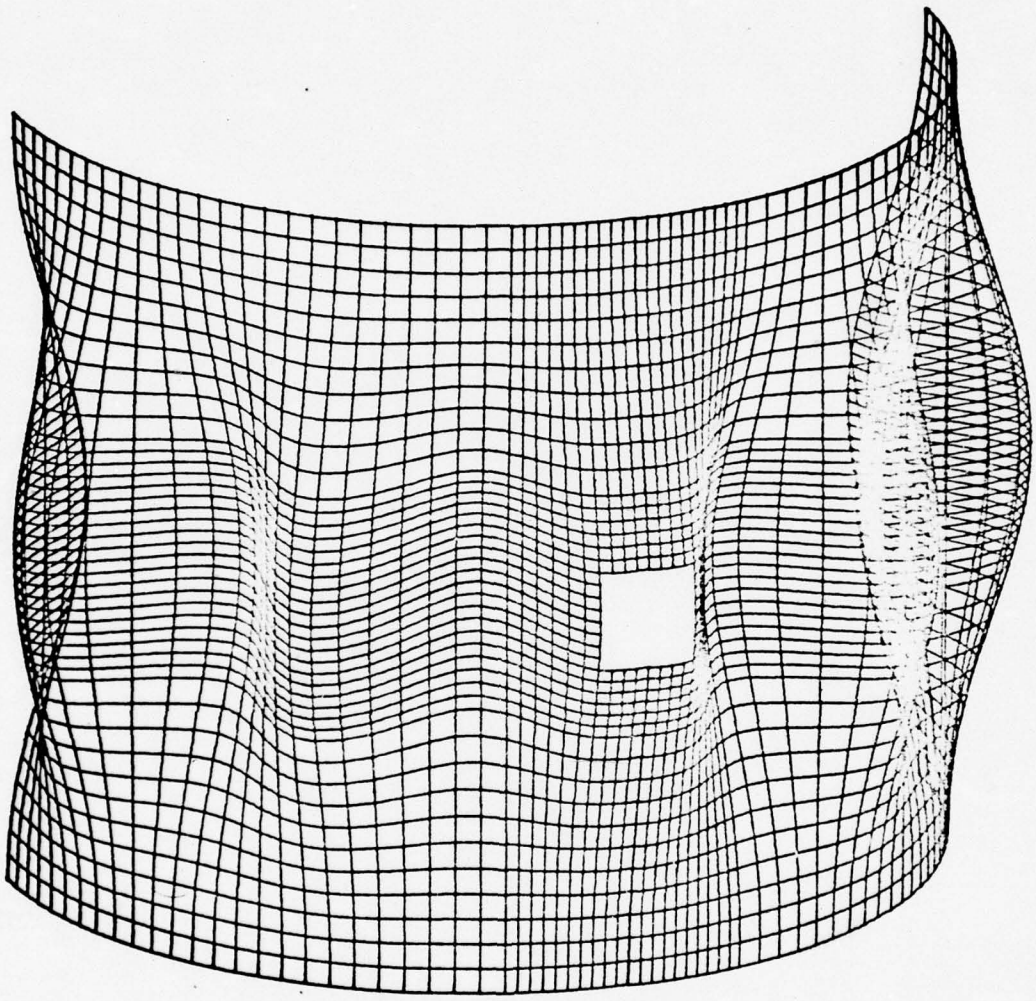


Figure 20. Normalized Buckling Displacements For a Stringer Stiffened Shell, 2a = 12"

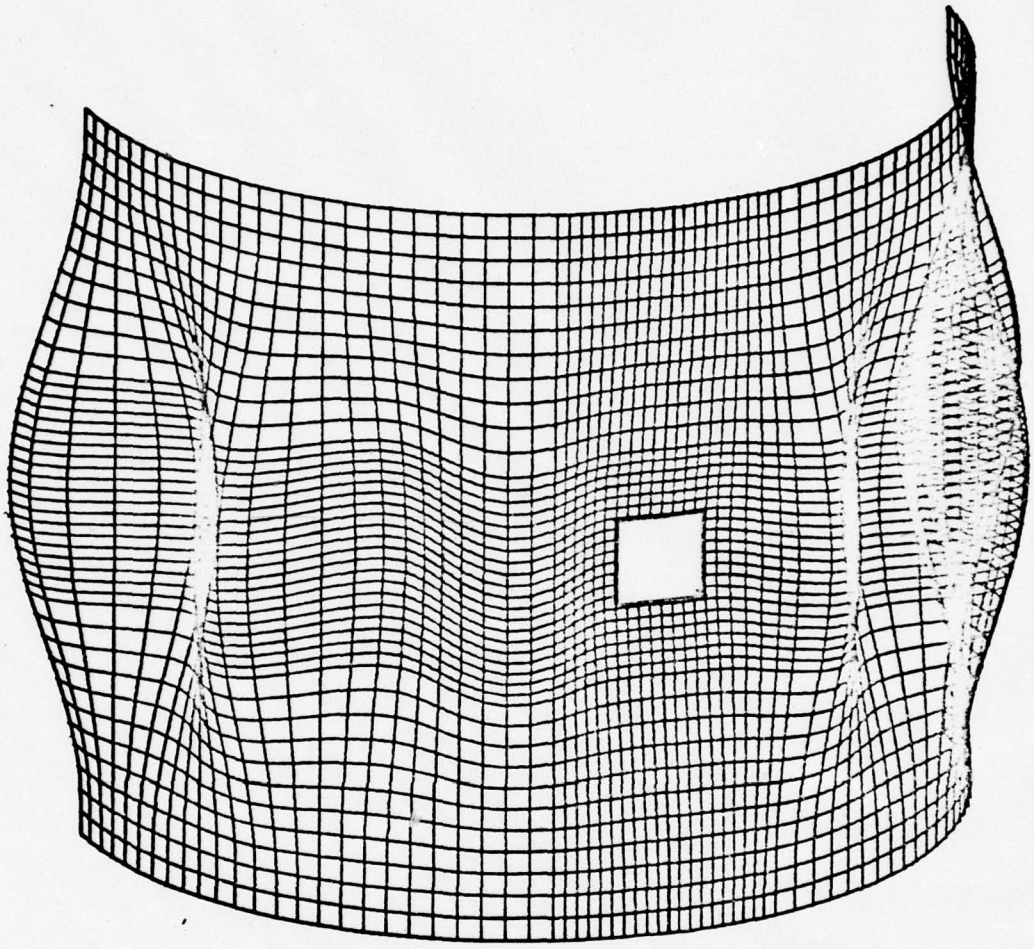


Figure 21. Normalized Buckling Displacements For Run 1

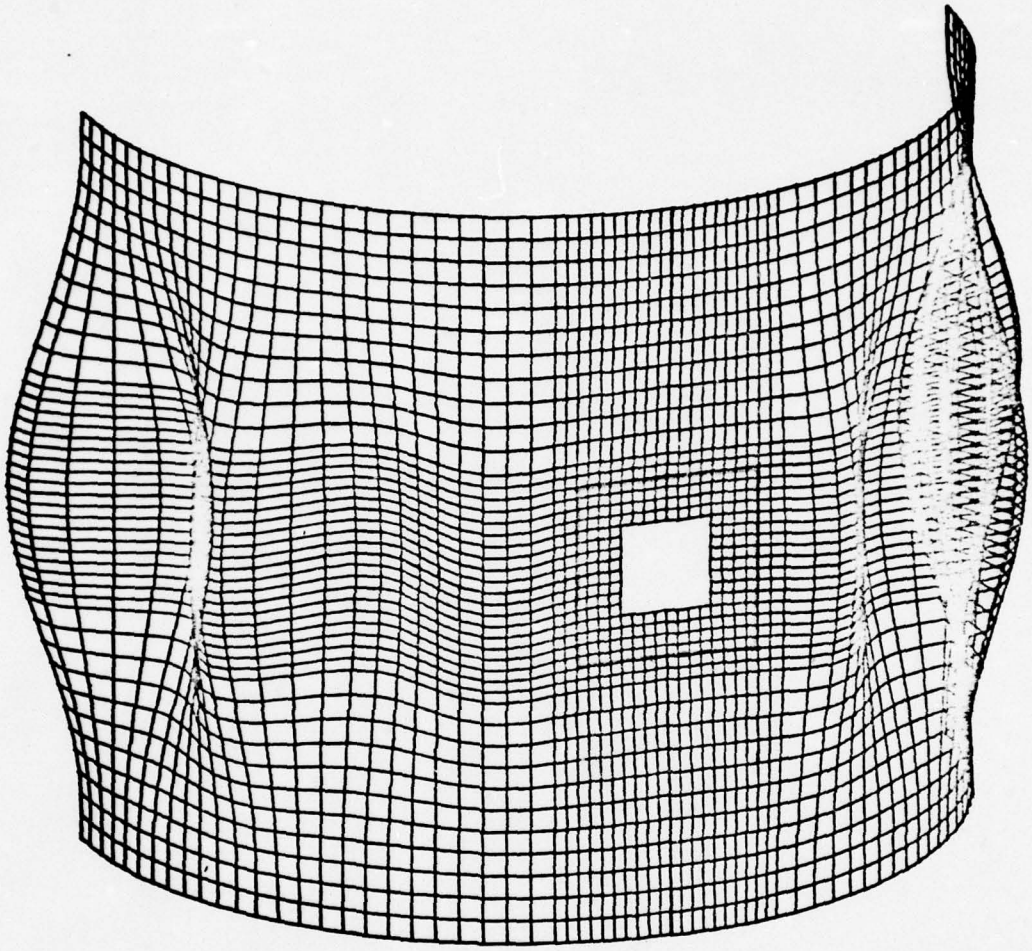


Figure 22. Normalized Buckling Displacements For Run 4

The normalized buckling displacements are shown in Figure 23. Notice that for this frame position, the buckling pattern no longer resembles the patterns for frame positions 1 and 4; instead, the pattern is similar to that of the shell without a frame. Also, notice that the vertical leg of the frame lies at the bottom of an inward buckle. It is supposed that the eccentricity effect of the internal frame contributes to the early buckling of the shell due to the additional compressive stress caused by the frame's eccentricity leading to a less stable configuration.

In Figures 24 through 27 buckling load ratio P_{cr}/P_o is plotted versus volume ratio W_{sf}/W_o. The variation of shell stiffening and cutout size is in the same order as for Figures 8 through 11. As a general rule the heavier reinforcing frames (W_{sf}/W_o) lead to higher buckling ratios (P_{cr}/P_o). An exception to this trend is shown in Figure 26 for frame position 6. Notice that for stringer stiffened shells, (Figures 24 and 25) the light frames ($W_{sf}/W_o = .5$) produce a strengthening effect that is roughly independent of frame position. The effect of frame position does not become large until heavier frames are used. On the other hand, for ring and stringer stiffened shells (Figures 26 and 27) the effect of frame position is very large for light frames ($W_{sf}/W_o = .5$).

Apparently the light frames for ring and stringer stiffened shells are affecting a factor of buckling which is not significant in stringer stiffened shells. An

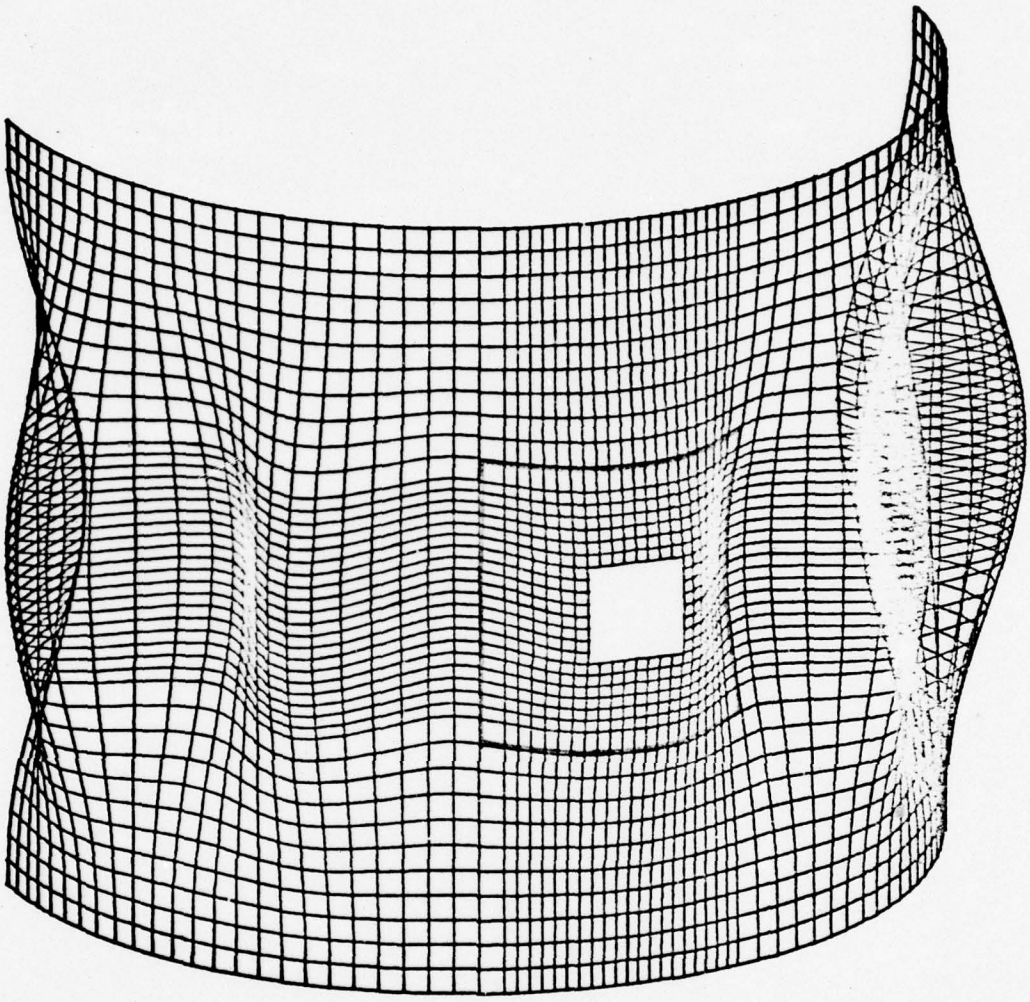


Figure 23. Normalized Buckling Displacements For Run 6

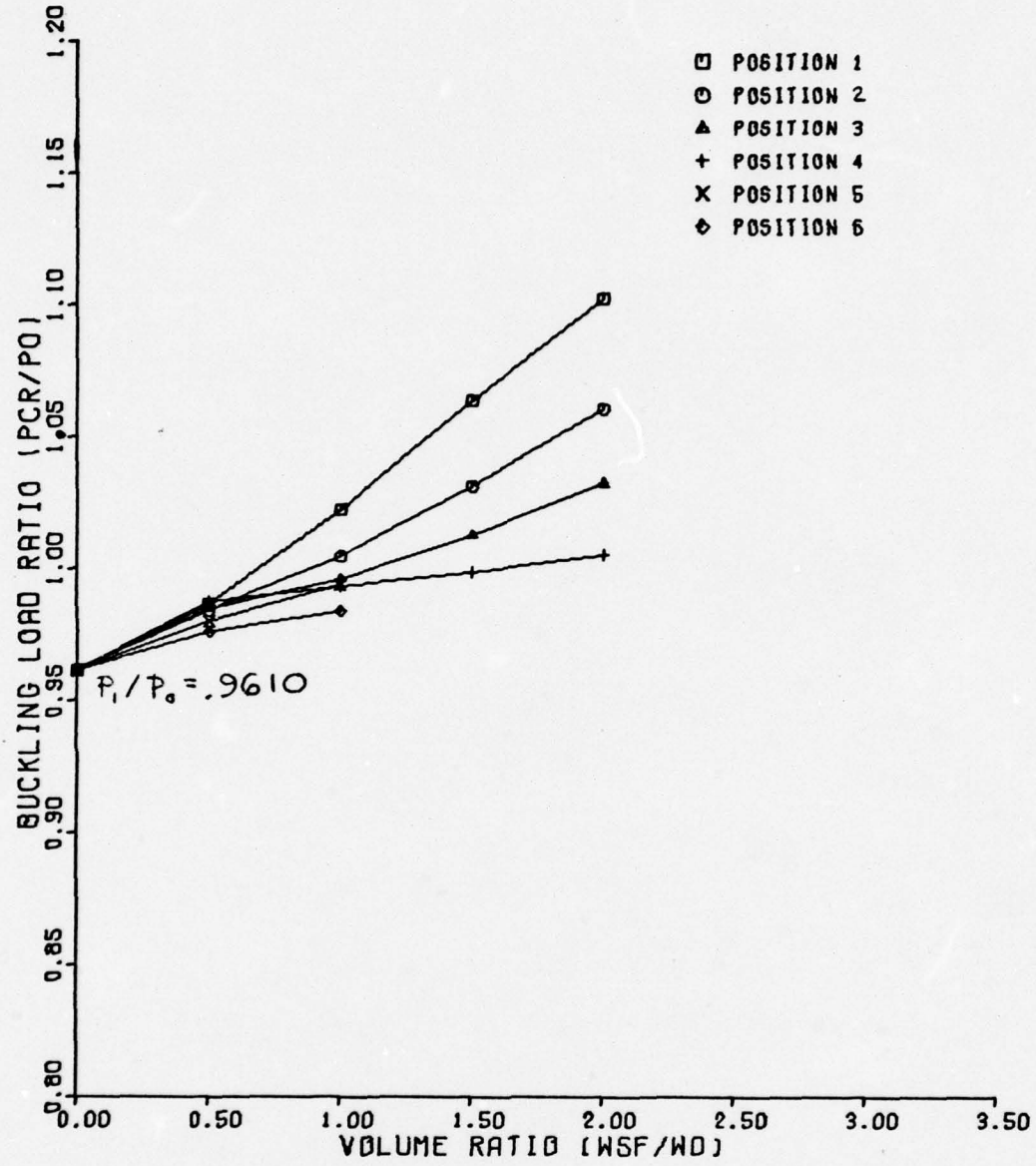


Figure 24. P_{cr}/P_o vs W_{sf}/W_o For a Stringer Stiffened Shell, 2a = 12"

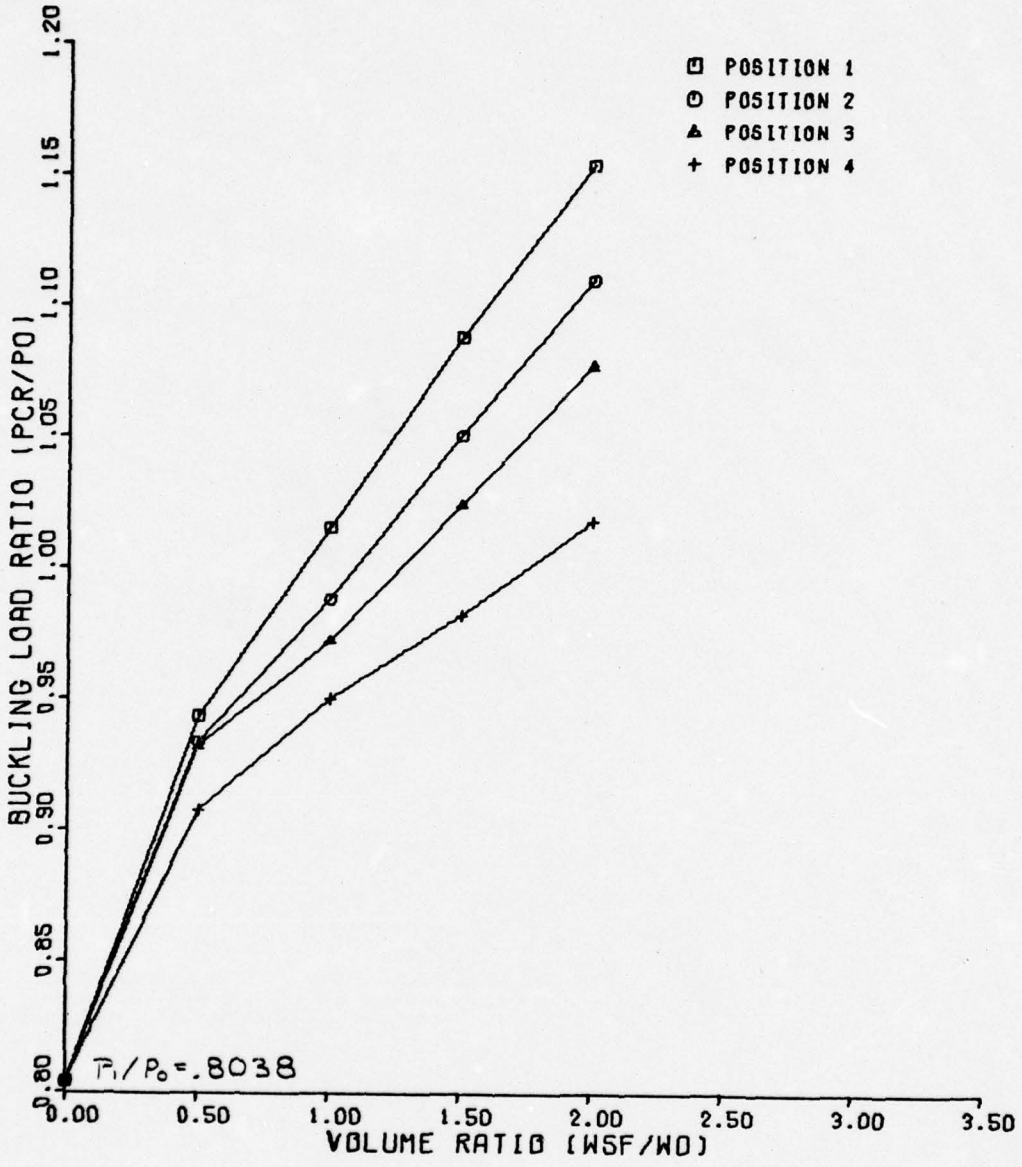


Figure 25. P_{cr}/P_o vs W_{sf}/W_o For a Stringer Stiffened Shell, 2a = 24"

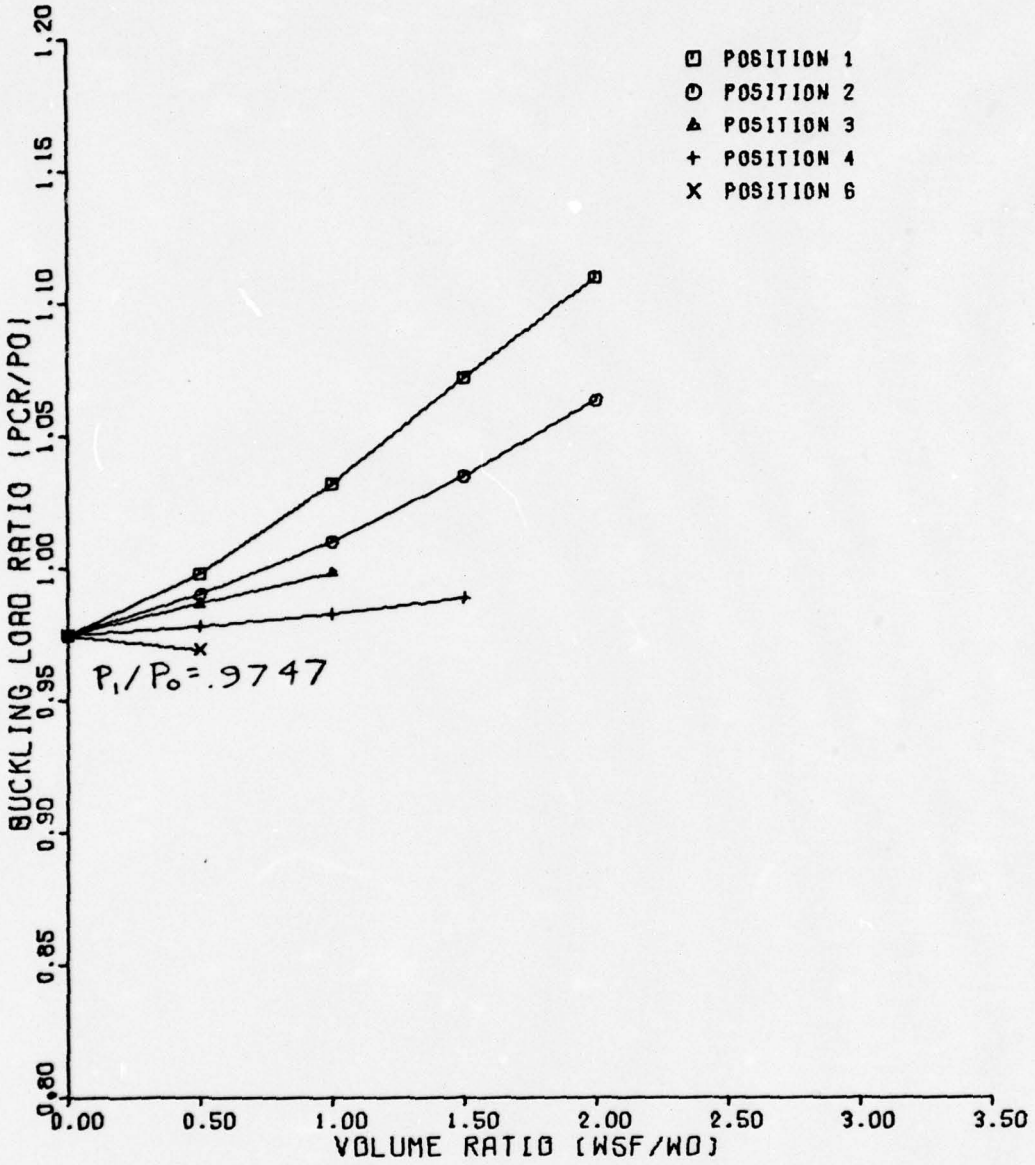


Figure 26. P_{cr}/P_o vs W_{sf}/W_o For a Ring and Stringer Stiffened Shell, 2a = 12"

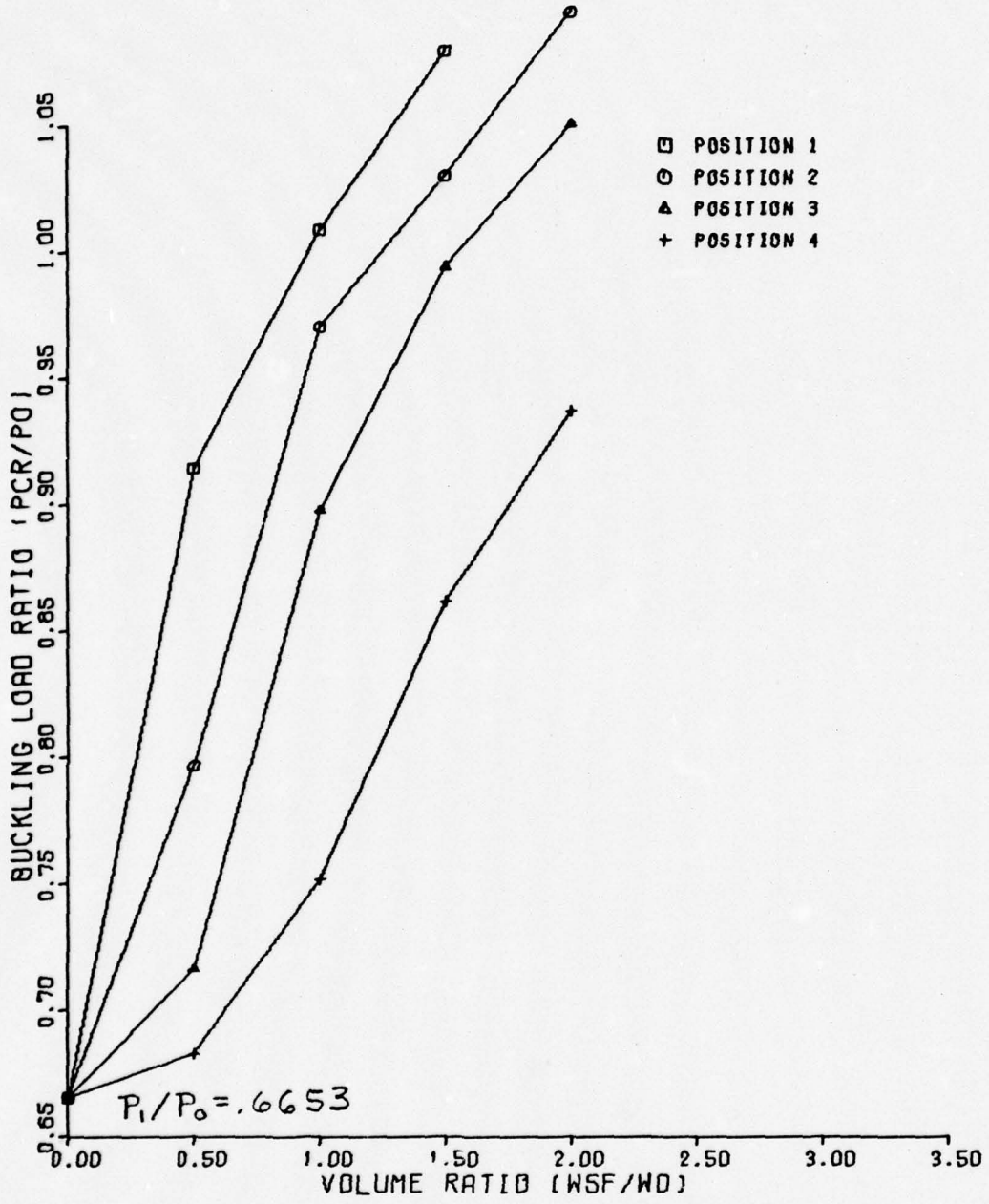


Figure 27. P_{cr}/P_o vs W_{sf}/W_o For a Ring and Stringer Stiffened Shell, 2a = 24"

interesting observation is that the ring and stringer stiffened shells already have a series of "reinforcing frames" surrounding the cutout consisting of the rings and stringers. The additional stiffness of this configuration requires heavier frames in order to alter the deformations significantly, whereas the relatively flexible stringer stiffened shell does not require heavy frames to alter the buckling pattern. In order to give a more detailed explanation of this effect, consider the stiffening effect of the ring of the reinforcing frame. Since the volume of reinforcing frame remains constant for a given volume ratio, W_{sf}/W_o, the cross-sectional area of the frame is inversely proportional to the distance, d, of the frame from the centerline of the cutout and the moment of inertia to the square of d. Hence, for the ring and stringer stiffened shell, the added stiffness of the reinforcing frame is large when the frame is along the cutout edge; but for the frame removed from the cutout it is not as large when compared to the stiffness of the existing ring stiffened skin. On the other hand, for the stringer stiffened shell, the relative increase in stiffness in the circumferential direction is large even for a frame removed from the cutout; since without the frame, only the relatively weak skin resists bending and compressive loads.

Note that Figure 24 through 27 can be used to determine the required combination of frame volume and frame location required to achieve a certain ratio P_{cr}/P_o. For example,

consider Figure 27 which is for a ring and stringer stiffened shell with a 24" x 24" cutout. Suppose that it is not possible to reinforce the cutout at the edge, but can be reinforced at position 2, what is the required volume of reinforcing frame to achieve a buckling load equivalent to a similar shell without a cutout? The required volume ratio of the reinforcing frame can be easily determined as follows. Draw a line through $P_{cr}/P_o = 1.0$ that intersects the frame position 2 curve. A line dropped from this intersection to the axis yields the required volume ratio (and therefore volume) for the reinforcing frame. Note that this procedure works equally well for any other value of P_{cr}/P_o.

IV. CONCLUSIONS

The following conclusions can be made.

(1) A reinforcing frame equal in volume to the material removed for a cutout and placed adjacent to that cutout, can increase the buckling load of the shell to or above that of a shell without a cutout.

(2) For either a stringer or a ring and stringer stiffened cylindrical shell with rectangular cutouts, the optimum position for a reinforcing frame is along the cutout edges.

(3) Positioning a frame away from the cutout edge, in most cases, drastically reduces the buckling load from that obtainable by placing the same volume of reinforcing frame adjacent to the cutout.

(4) For very light frames there may be a frame position away from the cutout edge which is equally effective as the position adjacent to the cutout.

(5) Frames positioned far away from the cutout edge may actually reduce the buckling load below that of an unreinforced shell.

(6) It is possible, with the use of STAGS to determine the reinforcement frame cross-section necessary to efficiently stiffen a shell with cutouts to any desired strength.

Bibliography

1. Hoff, N. J. "The Perplexing Behavior of Thin Cylindrical Shells Under Axial Compression". Israel J. Technol, Vol 4, pp. 1-28, 1966.

2. Timoshenko, S. P. and J. M. Gere. Theory of Elastic Stability (Second Edition). New York: McGraw-Hill Book Co., Inc., (1961).

3. Hoff, Nicholas J. "Buckling of Thin Shells". Proceedings of an Aerospace Scientific Symposium of Distinguished Lecturers in Honor of Theodore von Karmen on His 80th Anniversary. Institute of Aerospace Sciences, New York, p. 1, May 11, 1961.

4. Donnell, L. H. Stability of Thin-Walled Tubes Under Torsion. NACA Rep 479, 1933.

5. Almroth, B. O. and D. O. Brush. Buckling of Bars, Plates, and Shells. New York: McGraw-Hill Book Co., 1975.

6. Batdorf, S. B. A Simplified Method of Elastic Stability Analysis For Thin Cylindrical Shells. NACA Rep 874, 1947.

7. Donnell, L. H. "A New Theory For the Buckling of Thin Cylinders Under Axial Compression and Bending." Transactions of The American Society of Mechanical Engineers, Vol 56, p. 795, 1934.

8. Stein, Manuel. "Some Recent Advances in The Investigation of Shell Buckling." AIAA Journal, Vol 6, No. 12: 2339-2345 (December 1968).

9. Starnes, J. H., Jr. "The Effect of A Circular Hole On The Buckling of Cylindrical Shells." Ph.D Thesis, California Institute of Technology, Pasadena, Calif., 1970.

10. Singer, Josef. "Buckling of Integrally Stiffened Cylindrical Shells - a Review of Experiment and Theory," presented at Van Der Neut Symposium (1972).

11. Singer, J., M. Baruch and O. Harari. "On the Stability of Eccentrically Stiffened Cylindrical Shells under Axial Compression." Intl. J. Solids Structures, Vol 3, PP. 445-470, 1967.

12. Palazotto, A. N. "Bifurcation and Collapse Analysis of Stringer and Ring Stringer Stiffened Cylindrical Shells With Cutouts." Computers & Structures, Vol 7, pp. 47-58, 1977.

13. B. O. Almroth, F. A. Brogan, F. Zele. "User's Manual For the STAGS-A Computer Code." Collapse Analysis For Shells Of General Shape, Vol II. AFFDL-TR-71-8, March 1973.

14. Almroth, B. O., F. A. Brogan, M. B. Marlowe. "Analysis." Collapse Analysis For Shells of General Shape, Vol 1. AFFDL-TR-71-8, (August 1972).

15. Timoshenko, S. P.,J. N. Goodier. Theory of Elasticity (Third Edition). New York: McGraw-Hill Book Company, 1970.

16. Deschler, W. H. "Comparing Trigonometric and Conventional Finite Difference Approximations For Plate Buckling". Masters Thesis, Air Force Institute of Technology, WPAFB, OH., 1976.

17. Wylie, C. R. Advanced Engineering Mathematics (Fourth Edition) New York: McGraw-Hill Book Co., 1975.

18. Noble, B. Applied Linear Algebra. New York: Prentice-Hall, Inc., 1969.

19. MacNeal, R. H. The Nastran Theoretical Manual. NASA SP-221 (01). Washington, National Aeronautics and Space Administration, April, 1972.

Appendix A

Reinforcing Frame Geometric Parameters

The geometric parameters for the reinforcing frames depend upon the independent parameters; shell stiffening, cutout size, volume ratio, and frame position according to Eqs. (35-39). For completeness, the frame distance, d, cross-sectional area, A_{sf}, height h_{sf}, moment of inertia, I_{sf}, and torsional stiffness, GJ_{sf}, of the reinforcing frame are listed below for each run.

RUN	RINGS STRS	a	W_{sf}/W_o	POSI-TION	L_{sf}	A_{sf}	h_{sf}	I_{sf}	GJ_{sf}
1	STRS	6.0	.5	1	6.0	.28603	.53481	.00681758	43146.
2	STRS	6.0	.5	2	7.5	.22882	.47835	.00436325	27613.
3	STRS	6.0	.5	3	9.0	.19068	.43667	.00303004	19176.
4	STRS	6.0	.5	4	12.0	.14301	.37817	.00170440	10786.
5	STRS	6.0	1.0	1	6.0	.57205	.75634	.02727033	172583.
6	STRS	6.0	1.0	2	7.5	.45764	.67649	.01745301	110453.
7	STRS	6.0	1.0	3	9.0	.38137	.61755	.01212015	76703.
8	STRS	6.0	1.0	4	12.0	.28603	.53481	.00681758	43146.
9	STRS	6.0	1.5	1	6.0	.85808	.92633	.06135824	388311.
10	STRS	6.0	1.5	2	7.5	.68646	.82853	.03926927	248519.
11	STRS	6.0	1.5	3	9.0	.57205	.75634	.02727033	172583.
12	STRS	6.0	1.5	4	12.0	.42904	.65501	.01533956	97078.
13	STRS	6.0	2.0	1	6.0	1.14410	1.06963	.10908131	690330.
14	STRS	6.0	2.0	2	7.5	.91528	.95670	.06981204	441881.
15	STRS	6.0	2.0	3	9.0	.76274	.87335	.04848058	306813.
16	STRS	6.0	2.0	4	12.0	.57205	.75634	.02727033	172583.
17	STRS	12.0	.5	1	12.0	.57205	.75634	.02727033	172583.

RUN	RINGS STRS	a	W_{sf}/W_o	POSI-TION	L_{sf}	A_{sf}	h_{sf}	I_{sf}	GJ_{sf}
18	STRS	12.0	.5	2	13.5	.50849	.71309	.02154693	136361.
19	STRS	12.0	.5	3	15.0	.45764	.67649	.01745301	110453.
20	STRS	12.0	.5	4	18.0	.38137	.61755	.01212015	76703.
21	STRS	12.0	1.0	1	12.0	1.14410	1.06963	.10908131	690330.
22	STRS	12.0	1.0	2	13.5	1.01698	1.00846	.08618771	545446.
23	STRS	12.0	1.0	3	15.0	.91528	.95670	.06981204	441811.
24	STRS	12.0	1.0	4	18.0	.76274	.87335	.04848058	306813.
25	STRS	12.0	1.5	1	12.0	1.71616	1.31002	.24543296	1553243.
26	STRS	12.0	1.5	2	13.5	1.52547	1.23510	.19392234	1227253.
27	STRS	12.0	1.5	3	15.0	1.37293	1.17172	.15707709	994075.
28	STRS	12.0	1.5	4	18.0	1.14410	1.06963	.10908131	690330.
29	STRS	12.0	2.0	1	12.0	2.28821	1.51268	.43632526	2761320.
30	STRS	12.0	2.0	2	13.5	2.03396	1.42617	.34475082	2181784.
31	STRS	12.0	2.0	3	15.0	1.83057	1.35298	.27924817	1767245.
32	STRS	12.0	2.0	4	18.0	1.52547	1.23510	.19392234	1227253.
33	R&S	6.0	.5	1	6.0	.31463	.56092	.00824927	52206.
34	R&S	6.0	.5	2	7.5	.25170	.50170	.00527954	33412.

RUN	RINGS STRS	a	W_{sf}/W_o	POSI-TION	L_{sf}	A_{sf}	h_{sf}	I_{sf}	GJ_{sf}
35	R&S	6.0	.5	3	9.0	.20975	.45799	.00366634	23203.
36	R&S	6.0	.5	4	12.0	.15731	.39663	.00206232	13052.
37	R&S	6.0	1.0	1	6.0	.62926	.79326	.03299710	208825.
38	R&S	6.0	1.0	2	7.5	.50341	.70951	.02111814	133648.
39	R&S	6.0	1.0	3	9.0	.41951	.64769	.01466538	92811.
40	R&S	6.0	1.0	4	12.0	.31463	.56092	.00824927	52206.
41	R&S	6.0	1.5	1	6.0	.94389	.97154	.07424347	469856.
42	R&S	6.0	1.5	2	7.5	.75511	.86897	.04751582	300708.
43	R&S	6.0	1.5	3	9.0	.62926	.79326	.03299710	208825.
44	R&S	6.0	1.5	4	12.0	.47194	.68698	.01856087	117464.
45	R&S	6.0	2.0	1	6.0	1.25852	1.12184	.13198839	835299.
46	R&S	6.0	2.0	2	7.5	1.00681	1.00340	.08447257	534592.
47	R&S	6.0	2.0	3	9.0	.83901	.91597	.05866151	371244.
48	R&S	6.0	2.0	4	12.0	.62926	.79326	.03299710	208825.
49	R&S	12.0	.5	1	12.0	.62926	.79326	.03299710	208825.
50	R&S	12.0	.5	2	13.5	.55934	.74789	.02607178	164997.
51	R&S	12.0	.5	3	15.0	.50341	.70951	.02111814	133648.

RUN	RINGS STRS	a	W_{sf}/W_o	POSI-TION	L_{sf}	A_{sf}	h_{sf}	I_{sf}	GJ_{sf}
52	R&S	12.0	.5	4	18.0	.41951	.64769	.01466538	92811.
53	R&S	12.0	1.0	1	12.0	1.25852	1.12184	.13198839	835299.
54	R&S	12.0	1.0	2	13.5	1.11868	1.05768	.10428712	659990.
55	R&S	12.0	1.0	3	15.0	1.00681	1.00340	.08447257	534592.
56	R&S	12.0	1.0	4	18.0	.83901	.91597	.05866151	371244.
57	R&S	12.0	1.5	1	12.0	1.88777	1.37396	.29697388	1879424.
58	R&S	12.0	1.5	2	13.5	1.67802	1.29538	.23464603	1484977.
59	R&S	12.0	1.5	3	15.0	1.51022	1.22891	.19006328	1202831.
60	R&S	12.0	1.5	4	18.0	1.25852	1.12184	.13198839	835299.
61	R&S	12.0	2.0	1	12.0	2.51703	1.58652	.52795356	3341197.
62	R&S	12.0	2.0	2	13.5	2.23736	1.49578	.41714849	2639959.
63	R&S	12.0	2.0	3	15.0	2.01362	1.41902	.33789028	2138366.
64	R&S	12.0	2.0	4	18.0	1.67802	1.29538	.23464603	1484977.
65	STRS	6.0	.5	5	15.0	.11441	.33825	.00109081	6903.
66	STRS	6.0	.5	6	18.0	.09534	.30878	.00075751	4794.
67	STRS	6.0	1.0	5	15.0	.22882	.47835	.00436325	27613.
68	STRS	6.0	1.0	6	18.0	.19068	.43667	.00303004	19176.
82	R&S	6.0	.5	6	18.0	.10488	.32385	.00091659	5801.

Appendix B

Buckling Loads and Buckling Load Ratios

The buckling loads and the ratios of P_{cr}/P_o and P_{cr}/P, are listed below versus computer run number.

P_o	
STRS	R&S
-739275.	-1544810.

RINGS STRS	a	P_1	P_1/P_o
STRS	6	-710427.	.9610
STRS	12	-594257.	.8038
R&S	6	-1505686.	.9747
R&S	12	-1027689.	.6653

RUN	RINGS STRS	a	W_{sf}/W_o	POSI-TION	p_{cr}	p_{cr}/p_o	p_{cr}/p_1
1	STRS	6.	.5	1	-729443.	.9867	1.0268
2	STRS	6.	.5	2	-727416.	.9840	1.0239
3	STRS	6.	.5	3	-727975.	.9847	1.0247
4	STRS	6.	.5	4	-729944.	.9874	1.0275
5	STRS	6.	1.	1	-755997.	1.0226	1.0641
6	STRS	6.	1.	2	-742562.	1.0044	1.0452
7	STRS	6.	1.	3	-736492.	.9962	1.0367
8	STRS	6.	1.	4	-734463.	.9935	1.0338
9	STRS	6.	1.5	1	-786334.	1.0637	1.1068
10	STRS	6.	1.5	2	-762628.	1.0316	1.0735
11	STRS	6.	1.5	3	-748654.	1.0127	1.0538
12	STRS	6.	1.5	4	-738076.	.9984	1.0389
13	STRS	6.	2.	1	-814986.	1.1024	1.1472
14	STRS	6.	2.	2	-784170.	1.0607	1.1038
15	STRS	6.	2.	3	-763223.	1.0324	1.0743
16	STRS	6.	2.	4	-743344.	1.0055	1.0463
17	STRS	12.	.5	1	-697135.	.9430	1.1731
18	STRS	12.	.5	2	-690129.	.9335	1.1613
19	STRS	12.	.5	3	-688843.	.9318	1.1592
20	STRS	12.	.5	4	-670989.	.9076	1.1291
21	STRS	12.	1.	1	-750429.	1.0151	1.2628
22	STRS	12.	1.	2	-730447.	.9881	1.2292
23	STRS	12.	1.	3	-718609.	.9720	1.2093
24	STRS	12.	1.	4	-702140.	.9498	1.1815
25	STRS	12.	1.5	1	-804421.	1.0881	1.3537

RUN	RINGS STRS	a	W_{sf}/W_o	POSI-TION	p_{cr}	p_{cr}/p_o	p_{cr}/p_1
26	STRS	12.	1.5	2	-776607.	1.0505	1.3069
27	STRS	12.	1.5	3	-757189.	1.0242	1.2742
28	STRS	12.	1.5	4	-725810.	.9818	1.2214
29	STRS	12.	2.	1	-852897.	1.1537	1.4352
30	STRS	12.	2.	2	-820741.	1.1102	1.3811
31	STRS	12.	2.	3	-796221.	1.0770	1.3399
32	STRS	12.	2.	4	-752408.	1.0178	1.2661
33	R&S	6.	.5	1	-1541205.	.9977	1.0236
34	R&S	6.	.5	2	-1529239.	.9899	1.0156
35	R&S	6.	.5	3	-1524161.	.9866	1.0123
36	R&S	6.	.5	4	-1511143.	.9782	1.0036
37	R&S	6.	1.	1	-1594916.	1.032	1.0593
38	R&S	6.	1.	2	-1559540.	1.010	1.0358
39	R&S	6.	1.	3	-1542169.	.9983	1.0242
40	R&S	6.	1.	4	-1518237.	.9828	1.0083
41	R&S	6.	1.5	1	-1655584.	1.0717	1.0996
42	R&S	6.	1.5	2	-1598681.	1.0349	1.0618
43	R&S	6.	1.5	3			
44	R&S	6.	1.5	4	-1527205.	.9886	1.0143
45	R&S	6.	2.0	1	-1714487.	1.1098	1.1387
46	R&S	6.	2.0	2	-1642113.	1.0630	1.0906
47	R&S	6.	2.0	3			
48	R&S	6.	2.0	4			
49	R&S	12.	.5	1	-1412561.	.9144	1.3745
50	R&S	12.	.5	2	-1230672.	.7966	1.1975

RUN	RINGS STRS	a	W_{sf}/W_o	POSI-TION	p_{cr}	p_{cr}/p_o	p_{cr}/p_1
51	R&S	12.	.5	3	-1106145.	.7160	1.0763
52	R&S	12.	.5	4	-1054802.	.6828	1.0264
53	R&S	12.	1.	1	-1559507.	1.0095	1.5175
54	R&S	12.	1.	2	-1499013.	.9704	1.4586
55	R&S	12.	1.	3	-1387305.	.8980	1.3499
56	R&S	12.	1.	4	-1161682.	.7520	1.1304
57	R&S	12.	1.5	1	-1668644.	1.0802	1.6237
58	R&S	12.	1.5	2	-1600474.	1.0360	1.5574
59	R&S	12.	1.5	3	-1536190.	.9944	1.4948
60	R&S	12.	1.5	4	-1331873.	.8622	1.2960
61	R&S	12.	2.	1			
62	R&S	12.	2.	2	-1691898.	1.0952	1.6463
63	R&S	12.	2.	3	-1623268.	1.0508	1.5795
64	R&S	12.	2.	4	-1447692.	.9371	1.4087
65	STRS	6.	.5	5	-724668.	.9802	1.0200
66	STRS	6.	.5	6	-721550.	.9760	1.0157
67	STRS	6.	1.0	5	-734689.	.9938	1.0342
68	STRS	6.	1.0	6	-727661.	.9843	1.0243
82	R&S	6.	.5	6	-1497083.	.9691	.9943

VITA

James Anthony Cervantes was born on 28 August, 1947. He attended St. Xavier High School in Cincinnati, Ohio, and graduated from the University of Cincinnati with a Bachelor's Degree in Mechanical Engineering in May, 1970. Upon graduation he was employed by the Aeronautical Systems Division as an Aerospace Engineer at Wright Patterson Air Force Base. During his employment there, he was assigned to the F-15 System Program Office and later to the A-10 static test program. In 1975, he entered the School of Engineering, Air Force Institute of Technology.

Permanent Address:

4968 Woodman Park Drive
Apartment 3
Dayton, Ohio 45432

UNCLASSIFIED

SECURITY CLASSIFICATION OF THIS PAGE (When Data Entered)

REPORT DOCUMENTATION PAGE

READ INSTRUCTIONS BEFORE COMPLETING FORM

1. REPORT NUMBER: AFIT-GAE/MC/76D-2	2. GOVT ACCESSION NO. (Master's thesis,) 3. RECIPIENT'S CATALOG NUMBER
4. TITLE (and Subtitle): CUTOUT REINFORCEMENT OF STIFFENED CYLINDRICAL SHELLS.	5. TYPE OF REPORT & PERIOD COVERED: MS Thesis
	6. PERFORMING ORG. REPORT NUMBER
7. AUTHOR(s): James Anthony Cervantes	8. CONTRACT OR GRANT NUMBER(s)
9. PERFORMING ORGANIZATION NAME AND ADDRESS: Air Force Institute of Technology (AFIT/EN) Wright-Patterson AFB, Ohio 45433	10. PROGRAM ELEMENT, PROJECT, TASK AREA & WORK UNIT NUMBERS
11. CONTROLLING OFFICE NAME AND ADDRESS	12. REPORT DATE: March 1977
	13. NUMBER OF PAGES: 95 (296 p.)
14. MONITORING AGENCY NAME & ADDRESS (if different from Controlling Office)	15. SECURITY CLASS. (of this report): Unclassified
	15a. DECLASSIFICATION/DOWNGRADING SCHEDULE

16. DISTRIBUTION STATEMENT (of this Report)

Approved for public release; distribution unlimited

17. DISTRIBUTION STATEMENT (of the abstract entered in Block 20, if different from Report)

18. SUPPLEMENTARY NOTES

Approved for public release; IAW AFR 190-17

JERRAL F. GUESS, Captain, USAF
Director of Information

19. KEY WORDS (Continue on reverse side if necessary and identify by block number)

Cylindrical Shells
Stiffened Shells
Reinforced Shells
Shells with Cutouts

20. ABSTRACT (Continue on reverse side if necessary and identify by block number)

A study was carried out to determine the optimum placement and volume of a reinforcing frame around a cutout in an axially loaded stringer and ring and stringer stiffened cylindrical shell. The problem was analyzed using the linear bifurcation portion of STAGS (Structural Analysis of General Shells). Four parameters were varied; stringers versus rings and stringers, →

DD FORM 1 JAN 73 1473 EDITION OF 1 NOV 65 IS OBSOLETE

012225

UNCLASSIFIED

SECURITY CLASSIFICATION OF THIS PAGE (When Data Entered)

AD-A039 162 AIR FORCE INST OF TECH WRIGHT-PATTERSON AFB OHIO SCH--ETC F/G 13/13
CUTOUT REINFORCEMENT OF STIFFENED CYLINDRICAL SHELLS.(U)
MAR 77 J A CERVANTES

UNCLASSIFIED AFIT-GAE/MC/76D-2 NL

2 OF 2
ADA
039162



END

DATE
FILMED
5-77

cutout size, ratio of frame volume to cutout volume, and frame position. It appeared that in most cases the position with the frame next to the cutout edge was the most effective. This can be attributed to the frame's ability to delay the onset of local buckling. However, there was a relative maximum in the frame distance versus critical load curves for a frame positioned away from the cutout edge at a low ratio of frame to cutout volume.